LIBRARY
CALIFORNIA AIR RESOURCES BOARD
P.O. BOX 2815
SACRAMENTO, CA 95812

DESIGN FOR A NON-STEADY-STATE AIR QUALITY MODELING SYSTEM

April, 1987

by

Joseph S. Scire
Robert J. Yamartino
David G. Strimaitis
Steven R. Hanna

Document A025-201

Sigma Research Corporation
394 Lowell Street, Suite 12
Lexington, Massachusetts 02173

Prepared for

California Air Resources Board
1131 S Street
Sacramento, California 95814

Agreement No. A5-194-74

TD
883.1
S3
1987

Table of Contents

		Page
1.	Introduction	1-1
2.	Design of the Modeling System	2-1
3.	Input Data Processor Programs	3-1
4.	Meteorological Model	4-1
	4.1 Wind Field Model	4-1
	4.2 Micrometeorological Model	4-2
5.	Dispersion Model	5-1
	5.1 Solution of the Puff Equations	5-3
	5.2 Dispersion Coefficients	5-22
	5.3 Building Downwash	5-30
	5.4 Plume Rise	5-35
	5.5 Overwater and Coastal Dispersion	5-41
	5.6 Complex Terrain	5-47
	5.7 Dry Deposition	5-56
	5.8 Chemical Transformation	5-72
	5.9 Wet Removal	5-79
6.	Postprocessor Programs	6-1
REFERENCES		7-1

1. Introduction

Sigma Research Corporation has been awarded a contract by the California Air Resources Board (ARB) to design and develop a generalized non-steady-state air quality modeling system for the State of California. Systems Application, Incorporated (SAI) is a subcontractor to Sigma Research and has the responsibility of developing the wind field modeling component of the modeling system.

The ARB design specifications for the model include: (1) point and area source capabilities, (2) a modeling domain from tens of meters to hundreds of kilometers from the source, (3) predictions for averaging times ranging from one-hour to one year, (4) applicability to inert pollutants and those subject to linear removal and chemical conversion mechanisms, and, (5) applicability for rough or complex terrain situations.

This document and a companion report prepared by SAI on the wind field module outline the proposed modeling system. Special emphasis is placed on a description of the the key scientific modules which parameterize the transport, dispersion, chemical transformation, and removal processses necessary to meet the design objectives. These modules are described in sufficient detail to allow their evaluation by ARB.

Section 2 of this document describes the overall design of the modeling system and briefly summarizes the capabilities of each of the four major components: (1) the input data processors, (2) the meteorological model, (3) the dispersion model, and (4) the postprocessors. The individual preprocessing programs are described in Section 3. Section 4 contains a summary of the SAI recommendations for the wind field module and a description of the micrometeorological module. Each of the major modules composing the dispersion model is described in Section 5. Finally, Section 6 discusses the display and analysis capabilities of the postprocessors.

2. Design of the Modeling System

The basic design of the modeling package is shown in Figure 2-1. The proposed modeling system is divided into four subsustems: (1) input data preparation, (2) meteorological modeling, (3) dispersion modeling, and (4) postprocessing. At each step, the results of the modeling or data processing programs are stored on disk for future access or can be archived to magnetic tape. By dividing the modeling process into individual subtasks, certain potentially costly operations, such as the development of gridded wind fields, need not be repeated for each model application. For example, a processed meteorological data base can be developed for a selected area, archived, and then repeatedly applied to many different sources or source configurations. The dispersion modeling results can be easily re-scaled in inexpensive postprocessing operations to account for different emission rates (e.g., for different pollutants) or combined with the contributions of other sources.

The first phase consists of preparation of the meteorological, emissions, and geophysical data that is required by the meteorological and dispersion models. The meteorological data base includes hourly surface observations from NWS stations (TDF-14 format), twice-daily rawinsonde data (TD-6201 format), six-hourly winds derived from the Limited Fine Mesh (LFM) model of the National Meteorological Center (NMC), and depending of the application, actual or climatological land-sea temperature differences (for overwater/coastal situations), hourly precipitation observations (if wet removal is modeled), and hourly ozone measurements (for use in the SO_x/NO_x chemical transformation parameterization). Preprocessing capabilities will be provided for each data type. The functions of the preprocessors will include extraction, scanning, flagging, sorting, and if appropriate, correction or elimination of missing/invalid data. Preprocessing of the emissions data may include gridding of area source emissions data from an emissons inventory. The required geophysical data includes gridded land-use and/or roughness length data, terrain elevations, and optional Bowen ratio data. The functions of each of the data preparation programs are described in Section 3.

The second step in the modeling process involves the development of hourly gridded fields of micrometeorological parameters and winds required by the dispersion model. The meteorological model consists of a single program with two major modules: a wind field generator and a micrometeorological module. The recommended structure of the wind field generator consists of two modules: a simplified primitive-equation model for generation of the wind field on a coarse grid scale ($\sim$ 10 km), and a diagnostic model for interpolation of the coarse grid scale results down to a fine grid scale ($\sim$ 1 km). The structure of the wind field generator is summarized in Section 4.1. It is described in more detail in a companion document prepared by SAI. The micrometeorological model develops hourly gridded fields of the surface heat flux, momentum flux, mixing height, Monin-Obukhov length, and, if required precipitation rate. Section 4.2 contains a detailed description of the proposed algorithms for computation of

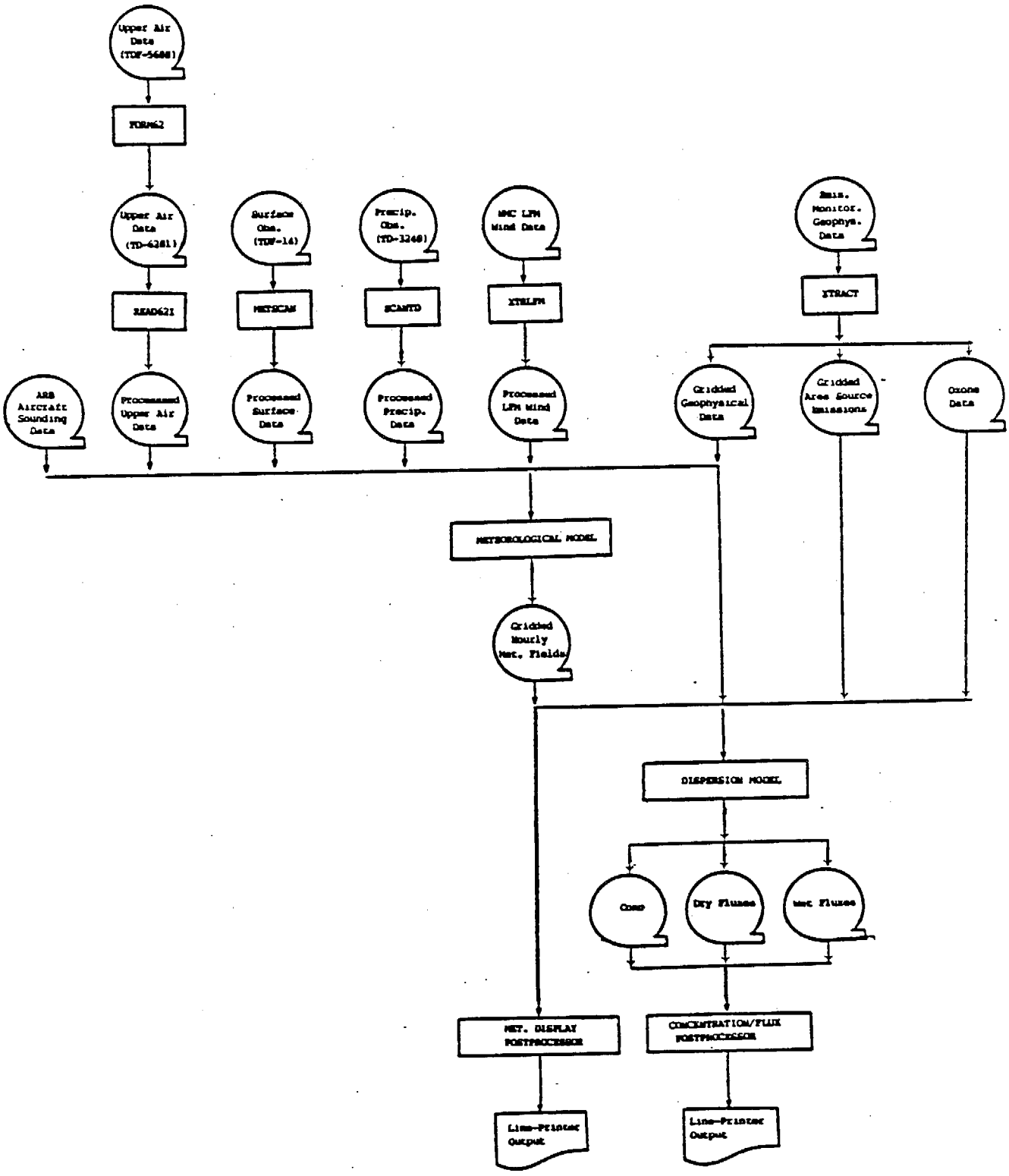

Figure 2-1. Proposed Non Steady-State Modeling System.

the micrometeorological parameters.

The dispersion modeling is performed as the third step in the modeling process. The dispersion model consists of a number of scientific modules for the treatment of puff advection and dispersion, building downwash effects, plume rise, overwater dispersion and coastal interaction effects, detailed subgrid-scale terrain effects, gas and particle dry deposition, linear chemical transformation, and wet pollutant scavenging. The model is design to allow, at user choice and when appropriate, several levels of sophistication in the treatment of the various processes, including options to completely by-pass modules that are unnecessary or not of interest for a particular application. The model is designed to be highly modular in order to facilitate potential future modification and update of the algorithms. Section 5 contains a detailed description of each of the proposed algorithms.

The final phase consists of the analysis, display, and reformatting of the concentration or deposition predictions produced by the dispersion model. The postprocessor, described in Section 6, includes modules for the time averaging (fixed and running averages), summing, scaling, and differencing of model output, source contribution analysis, peak concentration tabulation, file reformatting, and for gridded fields, line-printer plotting and statistical analysis of point-by-point or bulk differences.

Because of the potentially massive volume of data produced by the meteorological model, a second postprocessor will be provided to display user-selected subsets of the meteorological model output. For example, this program will allow a gridded meteorological variable such as the mixing height to be displayed for a selected time period or would allow all the variables at a particular grid point or subset of the grid area to be displayed. This capability is desirable to aid in the evaluation of the meteorological model as well as in the analysis of the dispersion results.

3. Input Data Processor Programs

The meteorological data inputs of the modeling system are designed to use standard tape deck formats available from the National Climatic Data Center (NCDC) or standard ARB file formats. However, due to modeling requirements, reformatting or preprocessing is necessary for several of the data inputs. In all cases, the data should be subject to quality assurance (QA) tests and screened for invalid, missing, or inappropriate data before use in the modeling. Some data preparation may also be required for the emissions, geophysical, and monitoring data sometimes required in the modeling.

This section discusses the set of data processing programs to accomplish these tasks that will be provided as part of the modeling package. Table 3-1 summarizes the input data requirements of the meteorological and dispersion models with the associated data processing programs appropriate for each of the data sets.

METSCAN - This program screens the routinely-available hourly surface observations from NWS stations for missing/duplicate or invalid data. The input format is the NCDC TDF-14 80-column format. The program performs QA checks on the wind speed, wind direction, temperature, opaque cloud cover, ceiling height, precipitation type, and relative humidity fields that are required in the meteorological model. Consistency checks are performed between the cloud cover and ceiling height variables.

READ62I - READ62I is an adaptation of an existing program that is part of the MESOPUFF II modeling package. It extracts the upper air data required by the meteorological model from a file in the current NCDC upper air data tape format (TD-6201) and checks for missing or incomplete data. The program will eliminate sounding levels with invalid data or when possible, fill in the missing variables by interpolation in height. Soundings which are totally or substantially missing are flagged for user action. The upper air output of READ62I is in a format convenient for possible editing by the user.

FORM62 - The NCDC has recently changed the format in which upper air sounding data is provided from TDF5600 format to TD-6201 format. In order to allow data in the older TDF5600 format to be included in the modeling, a program (FORM62) will provided to reformat TDF5600 data to TD-6201 format.

SCANTD - The NCDC hourly precipitation data format (TD-3240) contains data sorted by precipitation station (i.e., all time periods for a given station). The sequential dispersion model requires the

Table 3-1

Summary of Input Data Files and Associated Processor Routines

Data Type	Format/ Source	Parameters	Processor Program
Hourly surface met.	TDF-14 (NCDC)	Wind speed, wind direction, temperature, opaque cloud cover, ceiling height, precipitation type, relative humidity	METSCAN
Twice-daily upper air data	TD-6201 (NCDC)	Pressure, height, temperature, wind speed, wind direction	READ62I
Aircraft temperature soundings	ARB format (ARB)	Temperature from the surface to 7500 ft at 500 ft vertical intervals	FORM62
Hourly Precip.	TD-3240 (NCDC)	Precipitation rates	SCANTD
Misc.	Internal	Area source emissions, ozone monitoring data, geophysical data, land-sea temperature differences	XTRACT
Six-hourly LFM winds	Unspec. (NMC)	Gridded LFM wind speed and wind direction	XTRLFM

data sorted by time (i.e., precipitation for all stations at a given time). One function of SCANTD is to reorganize the data into the proper format. SCANTD also performs QA checks for missing or invalid precipitation data and resolves accumulation periods. An accumulation period is a time period during which the rain gauge has accumulated a known amount of precipitation but the time history of precipitation within the period is not known. SCANTD computes the average precipitation rate during the accumulation period and applies it to each of the accumulation hours.

XTRACT - This program extracts from a larger data base, the area source emissions, ozone monitoring data, geophysical data (land use, roughness length, terrain elevation) and land-sea temperature data inputs that, depending on the model application, may be required by the model. The area source option allows many small emission sources to be represented as an effective "area" source. The ozone measurements are used in the default SO_x/NO_x chemical transformation parameterization. A characterization of the surface characteristics (land use, roughness, etc.) is required by the meteorological model. Land-sea temperature differences are used in the determination of overwater/coastal turbulence and diffusion. The XTRACT program contains switches to control the type of data processed. A definition of the grid system to be used in the meteorological and dispersion modeling is required as input to XTRACT. The appropriate data is extracted from the data base and reformatted (ozone, temperature data) or gridded to the specifications of the inputs (geophysical, emissions data).

XTRLFM - XTRLFM processes the six-hourly wind output from the NMC LFM model. The program extracts the appropriate subset of the NMC tape data for the time period and grid region of interest for a particular run of the meteorological model. The meteorological grid system specification is an input to XTRLFM.

4. Meteorological Model

4.1 Wind Field Model

The proposed design for the wind field module is described in a companion document prepared by SAI entitled "Designing a Wind Field Module", and dated April, 1987. The report reviews existing mesoscale wind field models and discusses their applicability for the current project. The design criteria for the wind field model include the ability to depict, on a horizontal grid up to 100 km x 100 km with a minimum grid size of ~ 1 km, the following: land-sea breeze circulations, including the return flow aloft, thermally forced slope and valley-axis flow, including the return flow aloft, and the channeling of air flow by terrain. The recommended approach consists of two major components: (1) a hydrostatic primitive-equation (PE) prognostic mesoscale model; and (2) a diagnostic wind model.

Prognostic models generate mesoscale air flow patterns in response to differential surface heating and complex terrain, and are able to depict land-sea breeze and slope-valley circulations relatively accurately. However, on a fine grid scale, the computational requirements of such prognostic models are prohibitive. Diagnostic models are relatively inexpensive to run and have been shown to account for terrain-induced air flow channeling relatively well. However, diagnostic models have not been able to depict the return flow aloft associated with land-sea breeze or slope-valley circulations. Therefore, in order to provide a reasonable compromise between realistic representation of the mesoscale flow patterns and computational economy, the recommended approach consists of the following. A prognostic model, based on a version of the Colorado State University (CSU) 3-D Mesoscale Model, will provide wind fields on a coarse grid at 4 to 10 vertical levels. These wind fields will be available as "observations" to the diagnostic model, which generates the final wind field on the fine (e.g., one kilometer) grid scale. The diagnostic model will be a new code which will combine the desirable features of several existing diagnostic wind models. The diagnostic model applied in this way is expected to be able to represent the kinematic effects of terrain and slope flows on the fine scale.

However, both the prognostic and diagnostic models will be provided with the capability to be run on a stand-alone basis, without the other. The selection of the wind modeling approach will be based on the specific application, including factors such as the meteorological grid spacing and availability of observational data.

4.2 Micrometeorological Model

A number of significant advances have been made in recent years in our understanding and characterization of the structure of the planetary boundary layer (PBL) (e.g., see Weil, 1985; Briggs, 1985). As noted by van Ulden and Holtslag (1985) and others, an improvement in the quality of dispersion predictions can be expected from the use of the appropriate boundary layer scaling parameters. The principal parameters needed to describe the boundary layer structure are the surface heat flux (Q_h), surface momentum flux (ρu_*^2), and the boundary layer height (h). Several additional parameters, including the friction velocity (u_*), convective velocity scale (w_*), and the Monin-Obukhov length (L), are derived from these.

As part of the Electric Power Research Institute (EPRI) Advanced Plume project, Hanna et al. (1986) have evaluated several models for the prediction of these boundary layer parameters from "routinely"[1] available meteorological observations. Two basic methods are commonly used to estimate the surface heat and momentum fluxes. The first method is referred to as the profile method. It requires at a minimum the measurement of the wind speed at one height and the temperature difference between two heights in the surface layer, as well as knowledge of the air temperature and roughness characteristics of the surface. Monin-Obukhov similarity theory is then used to solve for the surface fluxes by iteration. The second approach, called the energy budget method, computes the surface heat flux by parameterizing the unkown terms of the surface energy budget equation.

Hanna et al. (1986) tested the following four energy budget models and two profile schemes:

Energy Budget Models

- Holtslag and van Ulden (1983)
- Weil and Brower (1983)
- Berkowicz and Prahm (1982)
- Briggs (1982)

---

[1] Temperature difference is not routinely reported at NWS meteorological stations. However, it typically is available at the many non-NWS sites with meteorological towers.

Profile Schemes

- Two-level tower method
- Four-level tower method

The major conclusion drawn from the comparison of the six schemes was that the energy budget methods were superior because of the sensitivity of the profile method to small errors in the measured temperature difference. However, as discussed below, this conclusion does not apply to the marine boundary layer, where a profile method based on the air-sea temperature difference is recommended. The relative performance of all of the energy budget methods was similar. An intercomparison of the u_* predictions of each of the energy budget methods showed a very high correlation with the other energy budget schemes (r^2 from 0.98 to 0.99 and RMS errors from 0.027 to 0.055 m/s). The correlation coefficient of the energy budget schemes with observed u_* ranged from 0.63 to 0.65 and RMS errors from 0.20 to 0.21 m/s.

A energy budget method, based primarily on Holtslag and van Ulden (1983), is recommended for application over land surfaces in the micrometeorological model. The energy balance at the surface can be written as:

$$Q_* + Q_f = Q_h + Q_e + Q_g \qquad (4.2\text{-}1)$$

where, Q_* is the net radiation (W/m^2),
Q_f is the anthropogenic heat flux (W/m^2),
Q_h is the sensible heat flux (W/m^2),
Q_e is the latent heat flux (W/m^2), and,
Q_g is the storage/soil heat flux term (W/m^2).

The ratio of the sensible heat flux to the latent heat flux is defined as the Bowen ratio.

$$B = \frac{Q_h}{Q_e} \qquad (4.2\text{-}2)$$

The model will require gridded values of the Bowen ratio. Seasonal default values, based on land use categories, will be provided. The Bowen ratio is important in determining the degree of convective turbulence because it reflects the partitioning of the available energy into sensible and latent heat flux. Typical values of B range from $\sim$ 0.1 over water bodies to $\geq$ 10 for deserts. In the summertime over parts of California, values of B $\sim$ 5-10 are expected.

The flux of heat into the soil or building materials, Q_g, is usually parameterized during the daytime in terms of the net radiation (e.g., Oke, 1978; Holtslag and van Ulden, 1983).

$$Q_g = c_g Q_* \tag{4.2-3}$$

where the constant c_g is a function of the properties of the surface. Oke (1982) suggests values for c_g of Ø.Ø5-Ø.25 for rural areas and Ø.25-Ø.3Ø for urban areas. The larger values for urban areas reflect the greater thermal conductivity and heat capacity of building materials. Holtslag and van Ulden (1983) use a value of Ø.1 for a grass covered surface.

The anthropogenic heat flux, Q_f, is a function of the population density and per capita energy usage. Oke (1978) summarizes annual and seasonally-averaged Q_f values for several urban areas. Although the Q_f term has been retained for generality, it is usually small compared to the other terms.

The net radiation, Q_*, is the residual of incoming (short-wave plus long-wave) radiation and outgoing (long-wave) radiation. Q_* can be expressed (Holtslag and van Ulden, 1973; Lansberg, 1981) as:

$$Q_* = Q_{sw} (1 - A) + Q_{lw-d} - Q_{lw-u} \tag{4.2-4}$$

where, Q_{sw} is the incoming short-wave radiation (W/m^2), consisting of a direct solar radiation term (Q_{sw-s}) plus a diffuse radiation term (Q_{sw-d}),
A is the albedo of the surface,
Q_{lw-d} is the incoming long-wave atmospheric radiation (W/m^2), and,
Q_{lw-u} is the long-wave radiation (W/m^2) emitted by the surface.

The method of Holtslag and van Ulden (1983) is used to estimate Q_*. The result of their parameterization of each of the terms in Equation (4.2-4) is:

$$Q_* = \frac{(1-A)Q_{sw} + c_1T^6 - \sigma T^4 + c_2N}{1 + c_3} \tag{4.2-5}$$

$$Q_{sw} = (a_1 \sin\phi + a_2)(1 + b_1 N^{b2}) \tag{4.2-6}$$

where, T is the measured air temperature (deg. K),

σ is the Stefan-Boltzmann constant (5.67×10^{-8} W/m^2/deg. K^4),
N is the fraction of the sky covered by clouds, and
ϕ is the solar elevation angle (deg.).

The last term in Equation (4.2-6) accounts for the reduction of incoming solar radiation due to the presence of clouds. The values for the empirical constants c_1, c_2, c_3, a_1, a_2, b_1, and b_2 suggested by Holtslag and van Ulden (1973) are used (see Table 4.2-1). The solar elevation angle is computed each hour using equations described by Scire et al. (1984).

Using Equations (4.2-1) to (4.2-6), the daytime sensible heat flux can be expressed in terms of only known quantities:

$$Q_h = \frac{B}{1 + B} \left[Q_*(1 - c_g) + Q_f \right] \qquad (4.2\text{-}7)$$

Once the sensible heat flux is known, the Monin-Obukhov length and surface heat flux are computed by iteration.

$$u_* = ku \left[\ln(z/z_o) - \psi_m(z/L) + \psi_m(z_o/L) \right] \qquad (4.2\text{-}8)$$

where z_o is the surface roughness length (m),
ψ_m is a stability correction function [e.g., see Dyer and Hicks (1970)],
k is the von Karman constant, and,
u is the wind speed (m/s) at height z.

The Monin-Obukhov length is defined as:

$$L = - \frac{\rho C_p T u_*^3}{k g Q_h} \qquad (4.2\text{-}9)$$

where T is the temperature (^{o}K), and,
g is the acceleration due to gravity (m/s^2).

Eqn. (4.2-8) is used to obtain an initial guess for u_* assuming neutral conditions ($L = \infty$). This value of u_* is used in Eqn. (4.2-9) to estimate L. A new value for u_* is then computed with Eqn. (4.2-8) and L. The procedure is repeated until convergence is obtained. Holtslag and van Ulden (1983) report that three iterations are usually sufficient.

During stable conditions, Weil and Brower (1983) compute u_* with the following method based on Venkatram (1980):

Table 4.2-1

Net Radiation Constants (Holtslag and van Ulden 1983)

Constant	Value
c_1	5.31×10^{-13} W/m^2/deg K^6
c_2	60 W/m^2
c_3	0.12
a_1	990 W/m^2
a_2	-30 W/m^2
b_1	-0.75
b_2	3.4

$$u_* = \frac{C_{DN}\, u}{2}\left[\, 1 + C^{1/2} \,\right] \qquad (4.2\text{-}10)$$

$$C = \frac{1 - 4u_o 2}{C_{DN}\, u^2} \qquad (C \geq 0) \qquad (4.2\text{-}11)$$

$$u_o^2 = \frac{\gamma z_m g \theta_*}{T} \qquad (4.2\text{-}12)$$

where C_{DN} is the neutral drag coefficient $[k/\ln(z_m/z_o)]$,
γ is a constant ($\pm$ 4.7), and,
z_m is the measurement height (m) of the wind speed, u.

The temperature scale, θ_*, is computed as the minimum of two estimates:

$$\theta_* = \min[\theta_{*1}, \theta_{*2}] \qquad (4.2\text{-}13)$$

The estimate of θ_* is based on Holtslag and van Ulden (1982):

$$\theta_{*1} = 0.09\ (1 - 0.5\ N^2) \qquad (4.2\text{-}14)$$

and θ_{*2} is:

$$\theta_{*2} = \frac{T\, C_{DN}\, u^2}{4\ \gamma z_m\, g} \qquad (4.2\text{-}15)$$

The heat flux is related to u_* and θ_* by:

$$Q_h = -\ \rho C_p\, u_*\, \theta_* \qquad (4.2\text{-}16)$$

and L is computed from Eqn. (4.2-9).

The daytime mixing height is computed using a modified Carson (1973) method based on Maul (1980). Knowing the hourly variation in the surface heat flux from Eqn. (4.2-7) and the vertical temperature profile from the twice-daily sounding data, the convective mixing height at time t+dt can be estimated

from its value at time t in a stepwise manner:

$$h_{t+dt} = \left[h_t^2 + \frac{2\, Q_h\, (1 + E)\, dt}{\psi_1\ C_p} + \frac{2\, d\theta_t\, h_t}{\psi_1} \right]^{1/2} + \frac{d\theta_{t+dt}}{\psi_1} \qquad (4.2\text{-}17)$$

$$d\theta_{t+dt} = \left[\frac{2\, \psi_1\, E\, Q_h\, dt}{\rho\ C_p} \right]^{1/2} \qquad (4.2\text{-}18)$$

where ψ_1 is the potential temperature lapse rate in the layer above h_t,
$d\theta$ is the temperature jump at the top of the mixed layer (^{o}K), and,
E is a constant ($\pm$ 0.15).

The potential temperature lapse rate is determined through a layer above the previous hour's convective mixing height. For daytime hours up to 2300 GMT, the morning (1200 GMT) sounding at the nearest upper air station is used to calculate ψ_1. After 2300 GMT, the afternoon sounding (0000 GMT) is used.

The neutral (mechanical) boundary layer height is estimated by Venkatram (1980) as:

$$h = \frac{B\, u_*}{[f\, N_B]^{1/2}} \qquad (4.2\text{-}19)$$

where f is the Coriolis parameter ($\pm$ 10^{-4} s^{-1})
B is a constant ($\pm$ $2^{1/2}$), and,
N_B is the Brunt-Vaisala frequency in the stable layer aloft.

The daytime mixing height is the maximum of the convective and mechanical values predicted by Eqns. (4.2-17) and (4.2-19).

In the stable boundary layer, mechanical turbulence production determines the vertical extent of dispersion. Venkatram (1980) provides the following empirical relationship to estimate the stable mixing height.

$$h = B_2\, u_*^{3/2} \qquad (4.2\text{-}20)$$

where B_2 is a constant ($\pm$ 2400).

In the convective boundary layer, the appropriate velocity scale is w_*, which can be computed directly from its definition using the results of Eqns. (4.2-8) and (4.2-17).

$$w_* = [\, g\, Q_h\, h\, /\, (T\, \rho\, C_p)\,]^{1/3} \qquad (4.2\text{-}21)$$

Over water, the aerodynamic and thermal properties of the surface require that different methods be used in the calculation of the boundary layer parameters. Some of the differences between the marine and continental boundary layers are described in Section 5.5. One of the most important differences is the absence of a large sensible heat flux driven by solar radiation. The method used in the OCD model (Hanna et al., 1985), which is based on a profile technique using the air-sea temperature difference and overwater wind speed, are recommended to compute the marine boundary layer parameters.

The neutral momentum drag coefficient over water, C_{uN}, can be expressed in terms of the 10-m wind speed (Garratt, 1977).

$$C_{uN} = (0.75 + 0.067\ u)\ 10^{-3} \qquad (4.2\text{-}22)$$

The friction velocity can then be determined from the definition of the drag coefficient:

$$u_* = u\ C_{uN}^{1/2} \qquad (4.2\text{-}23)$$

Because of the importance of the latent heat flux over water, virtual potential temperatures are used in the definition of the Monin-Obukhov length. Hanna et al. (1985) express L as:

$$L = \frac{\theta_v\ C_{uN}^{3/2}\ u^2}{E_2\ (\theta_v - \theta_{vs})} \qquad (4.2\text{-}24)$$

where θ_v, θ_{vs} are the virtual potential temperatures (^oK) of the air and water,
u is the 10-m wind speed (m/s), and,
E_2 is a constant (5.096×10^{-3}).

Over water, due to the effect of the wind on wave height, the surface roughness length varies. The OCD model employs a relationship derived by Hosker (1974) to express the surface roughness in terms of the 10 m wind speed:

$$z_o = 2.0 \times 10^{-6}\ u^{2.5} \qquad (4.2\text{-}25)$$

Hosker's result is based on the analysis of Kitaigorodskii (1973) showing $z_o \propto u_*^2$ and the logarithmic wind speed profile relating wind speed and u_*.

5. Dispersion Model

The ARB design specifications for the dispersion model include the capability for treating both point and area sources on spatial scales from tens of meters to hundreds of kilometers and time scales from one hour to one year. The model must include parameterizations for linear chemical reactions, wet and dry removal processes, and building downwash effects. In addition, the model must be applicable in overwater, coastal, and flat or complex terrain situations under a wide range of spatially-varying meteorological conditions.

Although the conventional Gaussian puff modeling approach offers many of the capabilities required for the ARB model, the puff model has traditionally been difficult to apply cost-effectively in the near-field of a source. Puff models generally require the release or sampling of many puffs (hundreds to thousands per hour) to adequately resolve a continuous plume close to a source (i.e., within a few hundred meters). In order to meet the broad design criteria, a hybrid circular/elongated puff approach is proposed that eliminates the near-field inefficiencies of the conventional puff model, while retaining its non steady-state capabilities. In the proposed approach, the emitted mass of pollutant from a source is modeled as a number of discrete packets or puffs (which may be circular or elongated). Each puff is independently subject to advection, depletion, and transformation processes. This gives the model a number of desirable properties that are well-suited for the ARB application.

- Ability to handle spatial variations in meteorological conditions, (e.g., changes in the wind field, stability, and turbulence properties of the atmosphere) such as may typically occur over tens of kilometers in flat terrain or over much shorter space scales in complex terrain and coastal regions.

- Ability to treat variability in the rate and characteristics of source emissions on time scales down to one hour or less. By packaging the emissions into a number of puffs, the causality relationship between emissions at the source and concentration at the receptor can be properly treated (i.e., the receptor does not "see" the impact of the emission before the puff has had time to be advected to the receptor or after it has passed by). Area source emissions can be modeled with puffs of non-zero initial size.

- Ability to handle low wind speed and calm conditions. The puff equation contains an along-wind diffusion term which replaces the inverse wind speed dependence in the steady-state plume equation.

- Ability to match Gaussian plume predictions under conditions where the plume assumptions are valid. The puff model can reproduce plume results during steady-state meteorological and emission conditions.

- Ability to accomodate modules for phenomena at the range of spatial scales of interest (tens of meters to hundreds of kilometers). The Gaussian puff framework can conveniently accomodate parameterization schemes for building downwash, plume rise, plume dispersion, removal processes, and chemical transformation that occur on a variety of spatial scales.

The subsections in this chapter describe the individual modules of the dispersion model including algorithms for the dispersion coefficients, building downwash, plume rise, overwater and coastal dispersion, complex terrain, dry deposition of particles and gases, chemical transformation, and wet removal. The basic forms and solution of the puff equations are discussed in the next section.

5.1 Solution of the Puff Equations

Puff models represent a continuous plume as a number of discrete packets of pollutant material. Most puff models (e.g., Ludwig et al., 1977; van Egmond and Kesseboom, 1983; Peterson, 1986) evaluate the contribution of a puff to the concentration at a receptor by a "snapshot" approach. Each puff is "frozen" at particular time intervals (sampling steps). The concentration due to the "frozen" puff at that time is computed (or sampled). The puff is then allowed to move, evolving in size, strength, etc. until the next sampling step. The total concentration at a receptor is the sum of the contributions of all nearby puffs averaged for all sampling steps within the basic time step. Depending on the model and the application, the sampling step and the time step may both be one hour, indicating only one "snapshot" of the puff is taken each hour.

A traditional drawback of the puff approach has been the need for the release of many puffs to adequately represent a continuous plume close to a source. Ludwig et al. (1977) have shown that if the distance between puffs exceeds a maximum of about 2 s_y, inaccurate results may be obtained (see Figure 2.1-1). Better results are obtained if the puff separation is reduced to no more than one s_y. If the puffs do not overlap sufficiently, the concentrations at receptors located in the gap between puffs at the time of the "snapshot" are underestimated, while those at the puff centers are overestimated.

Ludwig et al. (1977) recommend spacing puffs uniformly in space rather than in time with a puff merging/purging scheme to reduce the total number of puffs. Zannetti (1981) suggests tracking fewer puffs than necessary for adequate sampling, but then saturating the area near a receptor with artifically generated puffs to provide the required puff overlap (see Figure 2.1-2). Although both schemes act to reduce the number of puffs carried by the model, the snapshot sampling method still requires that an uneconomically large number of puffs be generated near the source. For example, at a receptor 100 meters from a source, and assuming PGT dispersion rates, puffs at a density corresponding to a release rate of over 1300 puffs/hour are required to meet the 2 s_y criterion for F stability, 3 m/s wind conditions. During high wind speed, neutral conditions (10 m/s, D stability), nearly 2200 puffs/hour are needed. The more stringent one s_y criterion would double the number of puffs required.

Two alternatives to the convential snapshot sampling function are discussed below. The first is based on the integrated sampling function in the MESOPUFF II model (Scire et al., 1984), with modifications for near-field applications. The second scheme uses a non-circular puff (slug) elongated in the direction of the wind to eliminate the need for frequent releases of puffs. The peformances of the original and modified integrated sampling functions and the slug model are evaluated for unsteady and steady-state conditions. The proposed sampling scheme for the ARB model is a hybrid circular puff/elongated slug method taking advantage of the strengths of each algorithm.

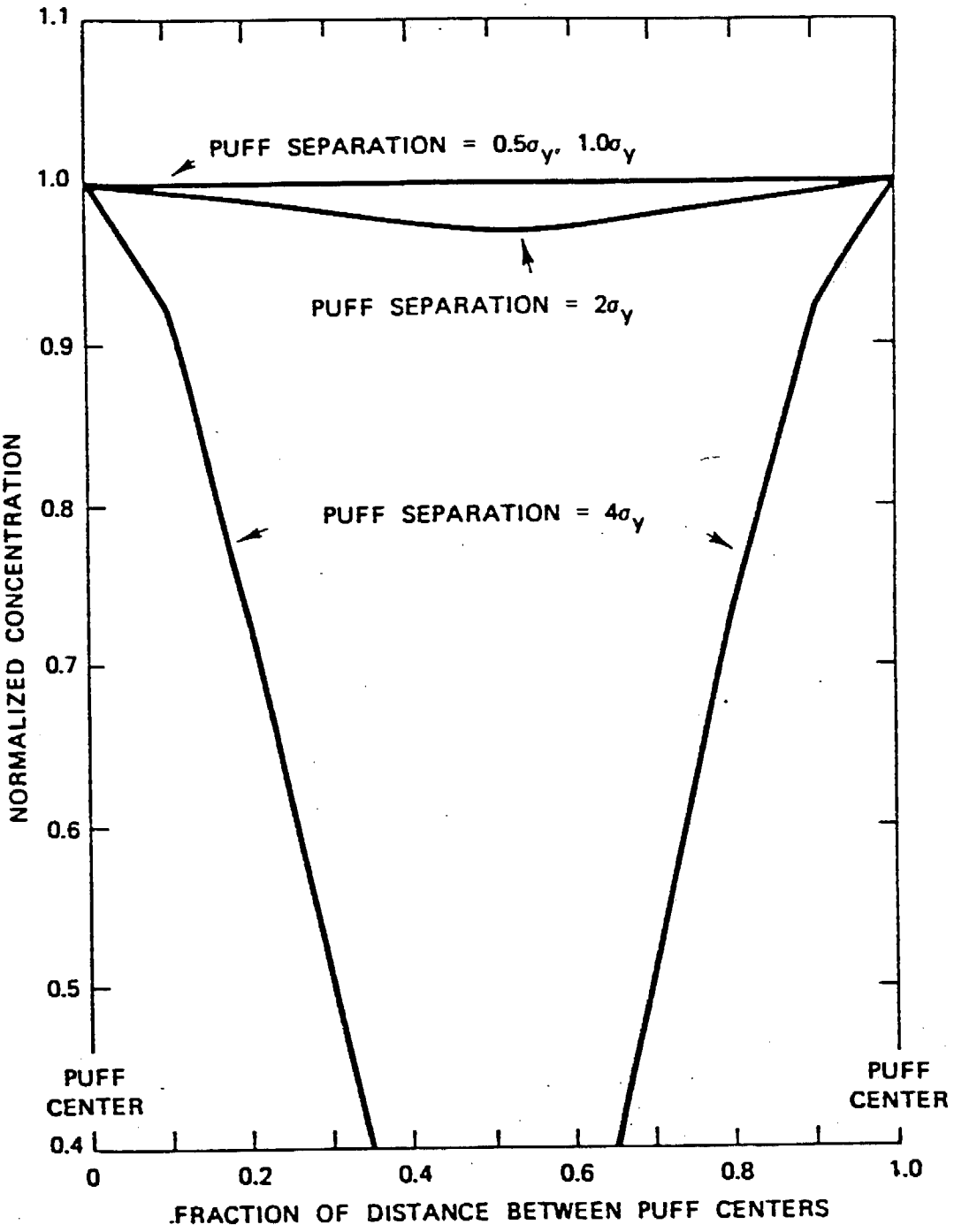

Figure 5.1-1. Normalized concentration between two puffs in a string of puffs of equal size and spacing. [From Ludwig et al. (1977)].

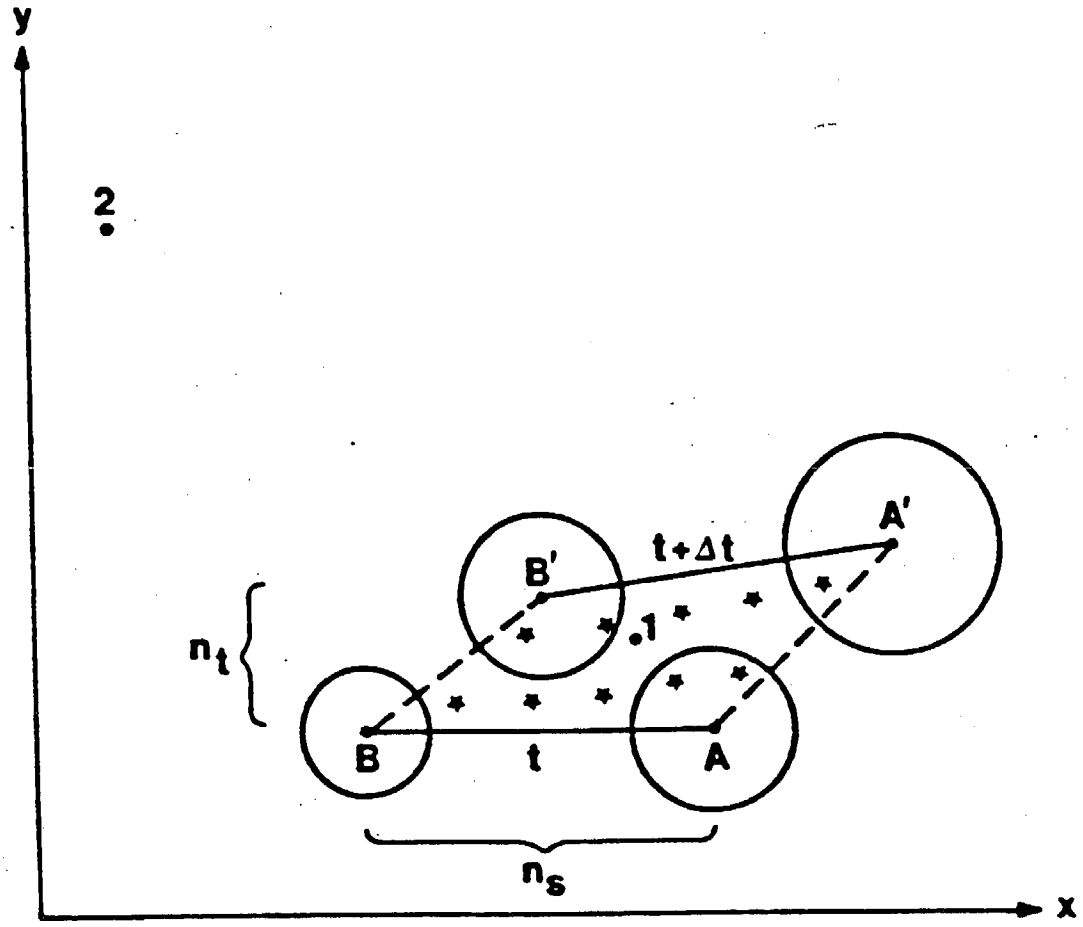

Figure 5.1-2. Illustration of the puff generation scheme of Zannetti (1981). The advected puffs (A -> A', B -> B') in the vicinity of Receptor 1 are not sufficient to resolve the plume. The mass from the original puffs is redistributed into n_t x n_s new puffs (asterisks) for sampling purposes. [From Zannetti (1981)].

INTEGRATED SAMPLING FUNCTION FORMULATION

The basic equation for the contribution of a puff at a receptor is:

$$C = \frac{Q}{2 \pi s_x s_y} g \exp\left[-d_a^2/(2s_x^2)\right] \exp\left[-d_c^2/(2s_y^2)\right] \qquad (5.1\text{-}1)$$

$$g = \frac{2}{(2\pi)^{1/2} s_z} \sum_{n=-\infty}^{\infty} \exp\left[-(H_e + 2nh)^2/(2s_z^2)\right] \qquad (5.1\text{-}2)$$

where C is the ground-level concentration (g/m^3),
Q is the pollutant mass (g) in the puff,
s_x is the standard deviation (m) of the Gaussian distribution in the along-wind direction,
s_y is the standard deviation (m) of the Gaussian distribution in the cross-wind direction,
s_z is the standard deviation (m) of the Gaussian distribution in the vertical direction,
d_a is the distance (m) from the puff center to the receptor in the along-wind direction,
d_c is the distance (m) from the puff center to the receptor in the cross-wind direction,
g is the vertical term (m) of the Gaussian equation,
H_e is the effective height (m) above the ground of the puff center, and,
h is the mixed-layer height (m).

The summation in the vertical term, g, accounts for multiple reflections off the mixing lid and the ground. It reduces to the uniformly mixed limit of 1/h for $s_z > 1.6$ h. In general, puffs within the convective boundary layer meet this criterion within a few hours after release.

For a horizontally symmetric puff, with $s_x = s_y$, Eqn. (5.1-1) reduces to:

$$C(s) = \frac{Q(s)}{2 \pi s_y^2(s)} g(s) \exp\left[-R^2(s)/(2s_y^2(s))\right] \qquad (5.1\text{-}3)$$

where R is the distance (m) from the center of the puff to the receptor, and,
s is the distance (m) traveled by the puff.

The distance dependence of the variables in Eqn. (5.1-3) is indicated (e.g., C(s), $s_y(s)$, etc.). Integrating Eqn. (5.1-3) over the distance of puff travel, ds, during the sampling step, dt, yields the time averaged concentration, $\bar{C}$.

$$\bar{C} = \frac{1}{ds} \int_{s_o}^{s_o+ds} \frac{Q(s)}{2 \pi s_y^2(s)} g(s) \exp [-R^2(s)/(2s_y^2(s))] \, ds \qquad (5.1\text{-}4)$$

where s_o is the value of s at the beginning of the sampling step.

If it is assumed that the most significant s dependencies during the sampling step are in the R(s) and Q(s) terms, an analytical solution to this integral can be obtained. Figure 5.1-3 illustrates the movement of a puff from coordinates (x_1,y_1) to (x_2,y_2). Assuming the trajectory segment is a straight line, and transforming s to a dimensionless trajectory variable, p, the radial distance to the receptor at (x_r,y_r) is:

$$R(s) = [(x_1 - x_r + p\, dx)^2 + (y_1 - y_r + p\, dy)^2]^{1/2} \qquad (5.1\text{-}5)$$

where p is zero at the beginning of the trajectory segment (i.e., at (x_1,y_1)), p is one at the end of the trajectory segment (i.e., at (x_2,y_2)), and, dx, dy are the incremental X and Y distances travelled by the puff (i.e., $dx = x_2-x_1$, and $dy = y_2-y_1$).

The exponential variation of Q due to removal and chemical transformation processes is expressed as a linear function of the sampling interval:

$$Q(s) = Q(s_o) + p\, [Q(s_o+ds) - Q(s_o)] \qquad (5.1\text{-}6)$$

Using Eqn. (5.1-6), and transforming to p coordinates, Eqn. (5.1-4) becomes:

$$\bar{C} = \frac{g}{2 \pi s_y^2} \left\{ Q(s_o) \int_0^1 \exp [-R^2(p)/(2s_y^2)] \, dp + \right.$$

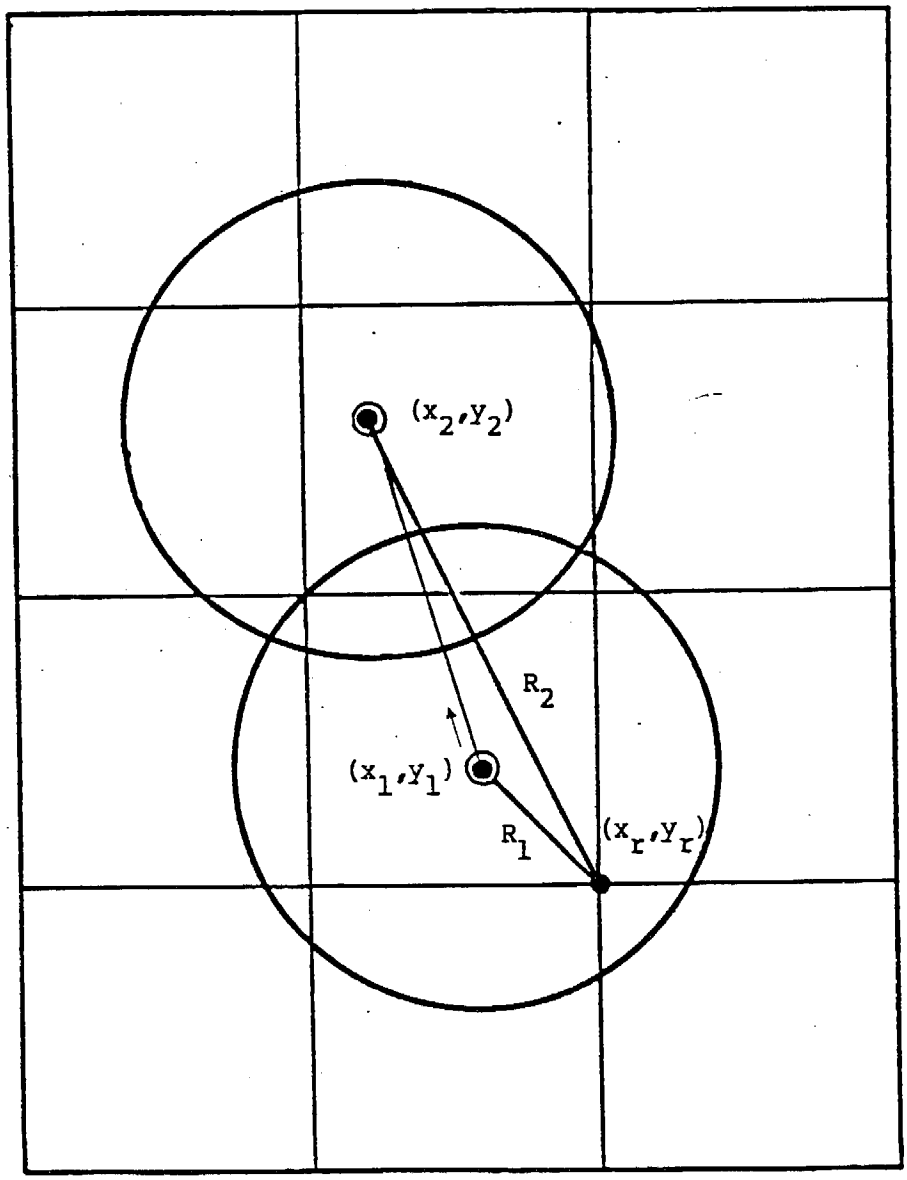

Figure 5.1-3. Illustration of the puff movement during the sampling step and the associated changes in the puff-receptor distance.

$$[Q(s_o+ds) - Q(s_o)] \int_{\emptyset}^{1} p \exp\left[-R^2(p)/(2s_y^2)\right] dp \Bigg\} \qquad (5.1\text{-}7)$$

The solution of the integrals in Eqn. (5.1-7) is expressed in terms of error functions and exponentials:

$$\bar{C} = \frac{g}{2\pi s_y^2} \{ Q(s_o) I_1 + [Q(s_o+ds) - Q(s_o)] I_2 \} \qquad (5.1\text{-}8)$$

$$I_1 = \left[\frac{\pi}{2a}\right]^{1/2} \exp\left[\frac{b^2}{2a} - \frac{c}{2}\right] \left\{ \operatorname{erf}\left[\frac{a+b}{(2a)^{1/2}}\right] - \operatorname{erf}\left[\frac{b}{(2a)^{1/2}}\right] \right\} \qquad (5.1\text{-}9)$$

$$I_2 = \frac{-b\, I_1}{a} + \frac{1}{a} \exp\left[\frac{b^2}{2a} - \frac{c}{2}\right] \left\{ \exp\left[\frac{-b^2}{a}\right] - \exp\left[\frac{a+2b+b^2}{2a}\right] \right\} \qquad (5.1\text{-}10)$$

$$a = (dx^2 + dy^2)/s_y^2 \qquad (5.1\text{-}11)$$

$$b = [dx\,(x_2-x_r) + dy\,(y_2-y_r)]/s_y^2 \qquad (5.1\text{-}12)$$

$$c = [(x_2-x_r)^2 + (y_2-y_r)^2]/s_y^2 \qquad (5.1\text{-}13)$$

The horizontal dispersion coefficient, s_y, and the vertical term, g, are evaluated and held constant throughout the trajectory segment. In MESOPUFF II, s_y and g are computed at the mid-point of the trajectory segment ($p = 0.5$). At mesoscale distances, the fractional change in the puff size during the sampling step is usually small, and the use of the mid-point values of s_y and g is adequate. This assumption reduces the number of times that the dispersion coefficients and vertical reflection terms need be computed to one per sampling step (independent of the number of receptors). This optimization for mesoscale distances, however, may not be appropriate in the near-field, where the fractional puff growth rate can be rapid and plume height may vary. For this reason, the integrated sampling function has been also tested with

receptor-specific values of s_y and g, evaluated at the point of closest approach of the puff to each receptor. The results of the test runs of both puff models as well as the slug model described in the next subsection are discussed below.

SLUG MODEL FORMULATION

In the slug model, the "puffs" consist of Gaussian packets of pollutant material stretched in the along-wind direction. As illustrated in Figure 5.1-4, a slug can be visualized as a group of overlapping circular puffs. The length of the main body of the slug is u dt_e, where u is the wind speed, and dt_e is the time of emission of the pollutant. The concentration due to the presence of a slug can be described as:

$$C(t) = \frac{F\,q}{(2\pi)^{1/2}\,u'\,s_y}\,g\left\{\exp\left[\frac{-d_c^2}{2\,s_y^2}\,\frac{u^2}{u'^2}\right]\right\} \qquad (5.1\text{-}14)$$

$$F = \frac{1}{2}\left\{\operatorname{erf}\left[\frac{d_{a2}}{(2)^{1/2}\,s_{y2}}\right] - \operatorname{erf}\left[\frac{-d_{a1}}{(2)^{1/2}\,s_{y1}}\right]\right\} \qquad (5.1\text{-}15)$$

where u is the vector mean wind speed (m/s),
u' is the scalar wind speed [defined as $u' = (u^2 + s_v^2)^{1/2}$ with s_v = wind speed variance],
q is the source emission rate (g/s), and,
F is a "causality" function.

Other variables have been defined previously. The subscripts 1 and 2 on the dispersion coefficients refer to values at the oldest and youngest ends of the slug, respectively. No numerical subscript indicates a value at the receptor.

This "slug" formulation retains many of the important properties of the circular puff model, while significantly reducing puff overlap problems associated with snapshot sampling of circular puffs. The concentration distribution within the body of the slug, away from the slug endpoints, approaches that of the Gaussian plume result under the appropriate steady-state conditions. The concentrations near the endpoints of the slug (both inside and outside of the body of the slug) fall off in such a way that if adjacent slugs

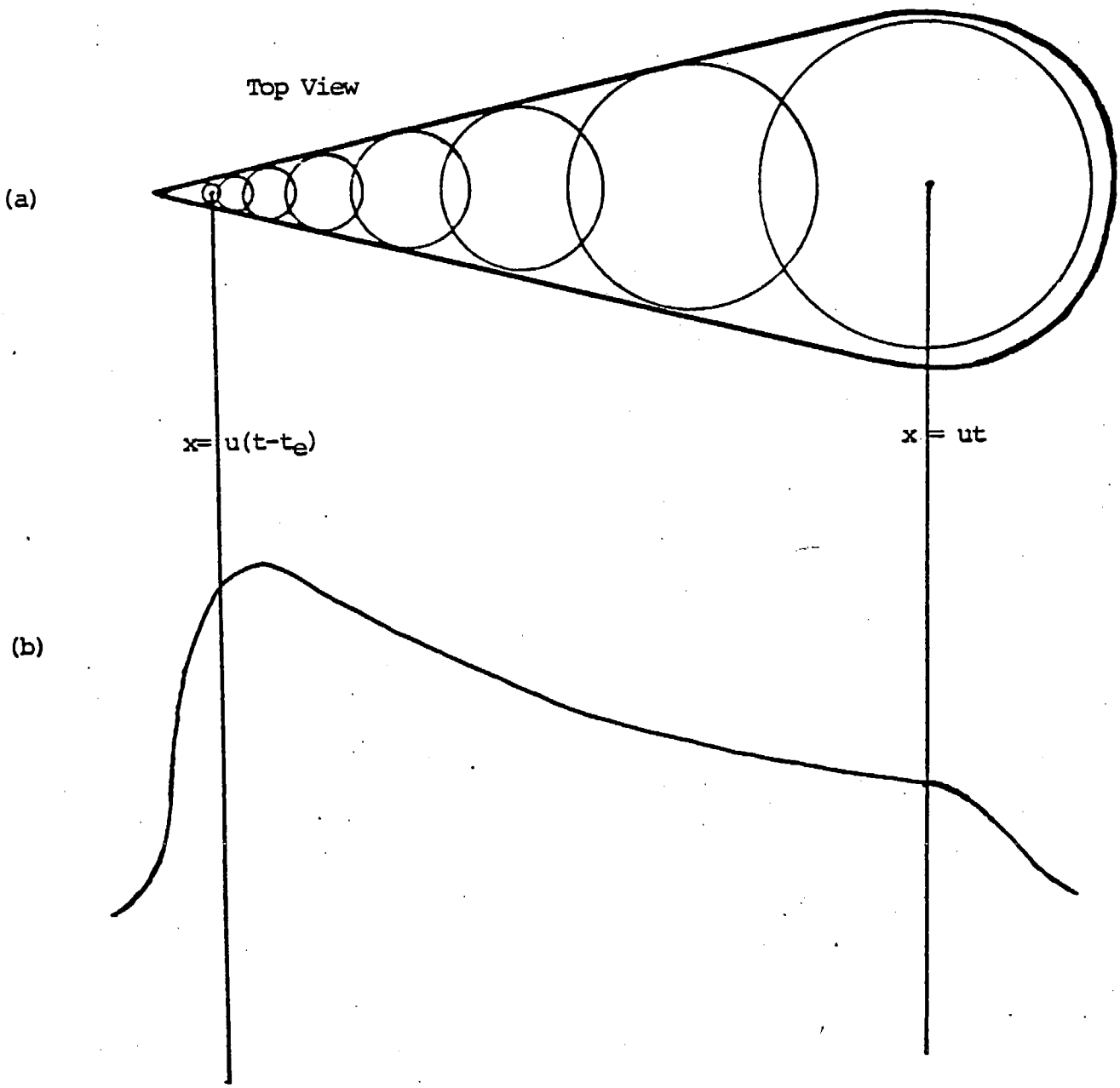

Figure 5.1-4. Schematic diagram showing multiple puff representation of a continuous point source. The outer envelope in (a) represents the solution given by Eqs. 5.1-14 and 5.1-15. Figure (b) is the accompanying concentration profile for for distribution.

are present, the plume predictions will be reproduced when the contributions of those slugs are included (again, during steady-state conditions). Eqn. (5.1-14) can be explicitly shown to conserve mass. As with circular puffs, each slug is independent, and is free to evolve in response to the local effects of dispersion, chemical transformation, removal, etc.

The "causality" function, F, accounts for edge effects near the endpoints of the slug. For long emission times such that $u\ dt_e >> s_x$, and points well inside the body of the slug, evaluation of the error functions in Eqn. (5.1-15) produces $F = 0.5\ (1 - (-1)) = 1$ (i.e., no edge effects). For receptors well outside the slug, F becomes zero, indicating that the pollutant material has not yet reached the receptor or has already passed it by. Near the endpoints, the causality factor produces a leading/trailing Gaussian tail on the distribution.

The factor (u/u') allows low wind speed and calm conditions to be properly treated. As u approaches zero, the exponential crosswind term becomes unity and F approaches $-\text{erf}\{d_a/[(2)^{1/2}\ s_y]\}/2$. Under these conditions, the radial concentration dependence of the distribution is determined by the causality factor. For u greater than a few meters per second, (u/u') is very close to one, so that this ratio becomes unimportant. The factors (u/u') and F make the slug model more "puff-like" than segmented plume models (e.g., Hales et al., 1977; Benkley and Bass, 1979). Unlike the slug model, segmented plume models generally do not properly treat low wind speed conditions or segment edge effects.

Eqn. (5.1-14) represents a "snapshot" description of the elongated puff at time t. As with the "snapshot" puff equation, Eqn. (5.1-14) must be integrated during the sampling step to produce a time-averaged concentration. In the case where the emission rate and meteorological conditions do not vary during the sampling step, a generalized analytical solution to the integral can be obtained for "emitting" slugs (i.e., the endpoint of the "youngest" end of the slug is at the source):

$$\overline{C}(t) = \frac{F\ q}{(2\pi)^{1/2}\ u'\ s_y}\ g \left\{ \exp\left[\frac{-d_c^2}{2\ s_y^2} \frac{u^2}{u'^2} \right] \right\} \qquad (5.1\text{-}16)$$

$$\overline{F} = \frac{1}{2}\ \text{erf}\ (\xi_2) + \frac{1}{2} \frac{(2)^{1/2}\ s_y}{u\ dt_s} \left\{ [\xi_2\ \text{erf}\ (\xi_2) - \xi_1\ \text{erf}\ (\xi_1)] \right.$$

$$\left. + \frac{1}{(1/2)} [\exp\ (\xi_2^2) - \exp\ (\xi_1^2)] \right\} \qquad (5.1\text{-}17)$$

$$\xi_1 = \frac{-d_{a1}}{(2)^{1/2}\, s_{y1}} \qquad (5.1\text{-}18)$$

$$\xi_2 = \frac{d_{a2}}{(2)^{1/2}\, s_{y2}} \qquad (5.1\text{-}19)$$

where dt_s is the sampling step (s).

For Eqn. (5.1-16) to apply, the sampling interval must correspond to the emission interval, as is normally the case for fresh emissions. The value of s_{y2} used is the initial lateral spread (if any) of the emissions at the source. For older slugs, the endpoint of the slug is no longer fixed at the source and the long axis of the slug is not likely to be along the advecting wind direction. An analytical integration of Eqn. (5.1-14) is not possible for these slugs unless restrictive conditions are imposed on the form of the puff growth equations. Because of the importance of generality in the puff growth equations, the time-averaged concentrations of older slugs are determined by numerical integration of Eqn. (5.1-14). As discussed in the next subsection, this can be accomplished with reasonable cost.

MODEL TESTING

The slug model and two versions of the integrated (circular) puff model have been subjected to several sensitivity tests in order to:

- evaluate the performance of each formulation in reproducing the known steady-state plume solution under the appropriate emission and meteorological conditions;
- demonstrate and intercompare the models' capabilities under non-steady conditions;
- assess the cost-effectiveness of the different algorithms;
- demonstrate the consistency of the circular puff/elongated slug models and the feasibility of the proposed hybrid approach.

Tables 5.1-1 (a,b) and 5.1-2 (a,b) present the plume, puff, and slug results for two sets of steady-state emission and meteorological conditions.

Table 5.1-1 (a)

Comparison of Plume, Puff, and Slug Models for Steady-State Conditions

(Wind Speed: 10 m/s, Stability Class: D, Stack Height: 10 m,
Unlimited Mixing Height, Emission Rate: 1 g/s)

Distance	Plume Model	Puff Model #1		
		100 puffs/hr	300 puffs/hr	500 puffs/hr
(m)	(g/m^3)	100 samp./hr	300 samp./hr	500 samp./hr
100	8.273×10^{-5}	1.266×10^{-4}	1.749×10^{-4}	9.618×10^{-5}
200	1.204×10^{-4}	1.266×10^{-4}	1.295×10^{-4}	1.306×10^{-4}
300	8.270×10^{-5}	1.288×10^{-4}	8.341×10^{-5}	7.929×10^{-5}
400	5.711×10^{-5}	3.164×10^{-5}	5.183×10^{-5}	5.682×10^{-5}
500	4.145×10^{-5}	3.693×10^{-5}	3.976×10^{-5}	4.176×10^{-5}
600	3.144×10^{-5}	3.733×10^{-5}	3.212×10^{-5}	3.145×10^{-5}
700	2.469×10^{-5}	3.189×10^{-5}	2.529×10^{-5}	2.467×10^{-5}
800	1.995×10^{-5}	1.559×10^{-5}	2.002×10^{-5}	1.995×10^{-5}
900	1.648×10^{-5}	1.658×10^{-5}	1.644×10^{-5}	1.648×10^{-5}
1000	1.387×10^{-5}	1.654×10^{-5}	1.394×10^{-5}	1.393×10^{-5}
2000	4.863×10^{-6}	4.871×10^{-6}	4.853×10^{-6}	4.856×10^{-6}
3000	2.616×10^{-6}	2.613×10^{-6}	2.614×10^{-6}	2.612×10^{-6}
4000	1.702×10^{-6}	1.704×10^{-6}	1.699×10^{-6}	1.698×10^{-6}
5000	1.219×10^{-6}	1.219×10^{-6}	1.217×10^{-6}	1.217×10^{-6}
6000	9.284×10^{-7}	9.280×10^{-7}	9.270×10^{-7}	9.268×10^{-7}
7000	7.374×10^{-7}	7.372×10^{-7}	7.364×10^{-7}	7.359×10^{-7}
8000	6.040×10^{-7}	6.029×10^{-7}	6.023×10^{-7}	6.022×10^{-7}
9000	5.066×10^{-7}	5.060×10^{-7}	5.055×10^{-7}	5.053×10^{-7}
10000	4.329×10^{-7}	4.326×10^{-7}	4.324×10^{-7}	4.321×10^{-7}
Compaq-286 CPU time (s)	1.0	249.4	2054.3	5592.4

Table 5.1-1 (b)

Comparison of Plume, Puff, and Slug Models for Steady-State Conditions

(Wind Speed: 10 m/s, Stability Class: D, Stack Height: 10 m, Unlimited Mixing Height, Emission Rate: 1 g/s)

Distance (m)	Plume Model (g/m^3)	Puff Model #2 (g/m^3)	Slug Model (g/m^3)
100	8.273×10^{-5}	8.273×10^{-5}	8.281×10^{-5}
200	1.204×10^{-4}	1.204×10^{-4}	1.205×10^{-4}
300	8.270×10^{-5}	8.270×10^{-5}	8.273×10^{-5}
400	5.711×10^{-5}	5.711×10^{-5}	5.712×10^{-5}
500	4.145×10^{-5}	4.145×10^{-5}	4.145×10^{-5}
600	3.144×10^{-5}	3.144×10^{-5}	3.143×10^{-5}
700	2.469×10^{-5}	2.469×10^{-5}	2.469×10^{-5}
800	1.995×10^{-5}	1.995×10^{-5}	1.995×10^{-5}
900	1.648×10^{-5}	1.648×10^{-5}	1.648×10^{-5}
1000	1.387×10^{-5}	1.387×10^{-5}	1.387×10^{-5}
2000	4.863×10^{-6}	4.863×10^{-6}	4.864×10^{-6}
3000	2.616×10^{-6}	2.616×10^{-6}	2.617×10^{-6}
4000	1.702×10^{-6}	1.702×10^{-6}	1.703×10^{-6}
5000	1.219×10^{-6}	1.219×10^{-6}	1.220×10^{-6}
6000	9.284×10^{-7}	9.284×10^{-7}	9.288×10^{-7}
7000	7.374×10^{-7}	7.374×10^{-7}	7.377×10^{-7}
8000	6.040×10^{-7}	6.040×10^{-7}	6.043×10^{-7}
9000	5.066×10^{-7}	5.066×10^{-7}	5.069×10^{-7}
10000	4.329×10^{-7}	4.329×10^{-7}	4.332×10^{-7}
Compaq-286 CPU time (s)	1.0	1.8	50.0

Table 5.1-2 (a)

Comparison of Plume, Puff, and Slug Models for Steady-State Conditions

(Wind Speed: 5 m/s, Stability Class: F, Stack Height: 10 m,
Unlimited Mixing Height, Emission Rate: 1 g/s)

Distance	Plume Model	Puff Model #1		
		100 puffs/hr	300 puffs/hr	500 puffs/hr
(m)	(g/m^3)	100 samp./hr	300 samp./hr	500 samp./hr
100	6.495×10^{-7}	1.379×10^{-7}	1.379×10^{-7}	5.814×10^{-5}
200	1.017×10^{-4}	1.823×10^{-4}	1.159×10^{-4}	1.018×10^{-4}
300	2.075×10^{-4}	1.869×10^{-4}	2.033×10^{-4}	2.046×10^{-4}
400	2.255×10^{-4}	2.171×10^{-4}	2.313×10^{-4}	2.242×10^{-4}
500	2.076×10^{-4}	2.234×10^{-4}	2.027×10^{-4}	2.078×10^{-4}
600	1.816×10^{-4}	1.733×10^{-4}	1.818×10^{-4}	1.813×10^{-4}
700	1.567×10^{-4}	1.736×10^{-4}	1.575×10^{-4}	1.566×10^{-4}
800	1.357×10^{-4}	1.337×10^{-4}	1.351×10^{-4}	1.355×10^{-4}
900	1.184×10^{-4}	1.197×10^{-4}	1.185×10^{-4}	1.183×10^{-4}
1000	1.042×10^{-4}	1.062×10^{-4}	1.041×10^{-4}	1.040×10^{-4}
2000	4.154×10^{-5}	4.135×10^{-5}	4.153×10^{-5}	4.154×10^{-5}
3000	2.397×10^{-5}	2.401×10^{-5}	2.398×10^{-5}	2.394×10^{-5}
4000	1.644×10^{-5}	1.644×10^{-5}	1.641×10^{-5}	1.641×10^{-5}
5000	1.224×10^{-5}	1.224×10^{-6}	1.223×10^{-5}	1.222×10^{-5}
6000	9.612×10^{-6}	9.609×10^{-6}	9.592×10^{-6}	9.594×10^{-6}
7000	7.830×10^{-6}	7.832×10^{-6}	7.822×10^{-6}	7.818×10^{-6}
8000	6.596×10^{-6}	6.584×10^{-6}	6.581×10^{-6}	6.580×10^{-6}
9000	5.669×10^{-6}	5.661×10^{-6}	5.659×10^{-6}	5.658×10^{-6}
10000	4.950×10^{-6}	4.945×10^{-6}	4.939×10^{-6}	4.940×10^{-6}
Compaq-286 CPU time (s)	1.1	309.8	2566.7	7049.5

Table 5.1-2 (b)

Comparison of Plume, Puff, and Slug Models for Steady-State Conditions

(Wind Speed: 5 m/s, Stability Class: F, Stack Height: 10 m,
Unlimited Mixing Height, Emission Rate: 1 g/s)

Distance (m)	Plume Model (g/m^3)	Puff Model #2 (g/m^3)	Slug Model (g/m^3) *
100	6.495×10^{-7}	6.495×10^{-7}	0.000×10^{-0}
200	1.017×10^{-4}	1.017×10^{-4}	1.018×10^{-4}
300	2.075×10^{-4}	2.075×10^{-4}	2.074×10^{-4}
400	2.255×10^{-4}	2.255×10^{-4}	2.255×10^{-4}
500	2.076×10^{-4}	2.076×10^{-4}	2.077×10^{-4}
600	1.816×10^{-4}	1.816×10^{-4}	1.817×10^{-4}
700	1.567×10^{-4}	1.567×10^{-4}	1.567×10^{-4}
800	1.357×10^{-4}	1.357×10^{-4}	1.357×10^{-4}
900	1.184×10^{-4}	1.184×10^{-4}	1.184×10^{-4}
1000	1.042×10^{-4}	1.042×10^{-4}	1.042×10^{-4}
2000	4.154×10^{-5}	4.154×10^{-5}	4.154×10^{-5}
3000	2.397×10^{-5}	2.397×10^{-5}	2.397×10^{-5}
4000	1.644×10^{-5}	1.644×10^{-5}	1.644×10^{-5}
5000	1.224×10^{-5}	1.224×10^{-5}	1.224×10^{-5}
6000	9.612×10^{-6}	9.613×10^{-6}	9.614×10^{-6}
7000	7.830×10^{-6}	7.830×10^{-6}	7.832×10^{-6}
8000	6.596×10^{-6}	6.596×10^{-6}	6.598×10^{-6}
9000	5.669×10^{-6}	5.669×10^{-6}	5.671×10^{-6}
10000	4.950×10^{-6}	4.950×10^{-6}	4.952×10^{-6}
Compaq-286 CPU time (s)	1.1	1.5	49.5

* The version of slug model used in the test runs assigns a zero concentration to receptors more than 3 s_z from plume centerline.

Plume centerline values are presented at receptors from 100 m to 10 km from the source. A constant emission rate of 1 g/s from a 10 m high source is assumed. The first set of results assume neutral (D class) stability conditions with 10 m/s winds. Stable (F class) conditions with 3 m/s winds are applied in the second set of runs. Puff model #1 employs the integrated puff sampling function with trajectory mid-point values of s_y and g. The puff release rate and sampling rate were varied from 100/hr to 500/hr for the puff model #1 simulations. Puff model #2 uses the same integrated sampling function as #1, except receptor-specific values of s_y and g are used instead of trajectory mid-point values. The puff release rate and sampling rate in the puff model #2 runs were both 1/hr. The slug model employs the time-integrated relationship (Eqn. 5.1-16) for the "youngest" slug originating at the source. A numerical integration of Eqn. (5.1-14) is performed for older slugs. (Numerical integration was not necessary in this special case of steady-state conditions, but was performed anyway to demonstrate the more general technique and allow its evaluation in terms of its consistency with the plume solution and its cost effectiveness).

The results indicate that a large number of puffs/samples are necessary to adequately reproduce the plume solution at near-field receptors when the puff model #1 assumptions are employed. The errors are associated with the use of the trajectory mid-point values of s_y and g. This model is optimized for source-receptor distances on scales from tens to hundreds of kilometers, and is not cost effective for application to close to the source. Puff model #2, using receptor-specific dispersion coefficients and the integrated sampling function, reproduces the plume solution exactly with a computational cost less than 1% of that required for puff model #1. In fact, its CPU requirements are competitive with those needed to solve the steady-state plume equation. The concentration predictions from the slug model also compare well with the steady-state plume solution. The CPU costs of the slug model, although higher than the puff model #2, are reasonably modest. Use of a more sophisticated integration scheme is likely to reduce the cost of the slug model further. Additional test runs of the puff and slug models under a range of different meteorological conditions produced similar results.

The slug and puff (#2) models were also used to simulate a case of non-steady emissions. An emission rate of 1 g/s for a duration of one hour was modeled. Although a one-hour release was used in this demonstration run, either model is capable of handling arbitrary variations in emission rates, including those on time scales of less than one hour. B stability, 1 m/s winds were the assumed meteorological conditions. The results are presented in Figures 5.1-5 and 5.1-6 along with the steady-state plume solution. The puff and slug model results intercompare well (within a few percent, except at the tails of the distribution with very low concentration values). The puff/slug predictions approach the steady-state results when the center of the pollutant cloud passes the receptor, but clearly show the causality and edge effects of

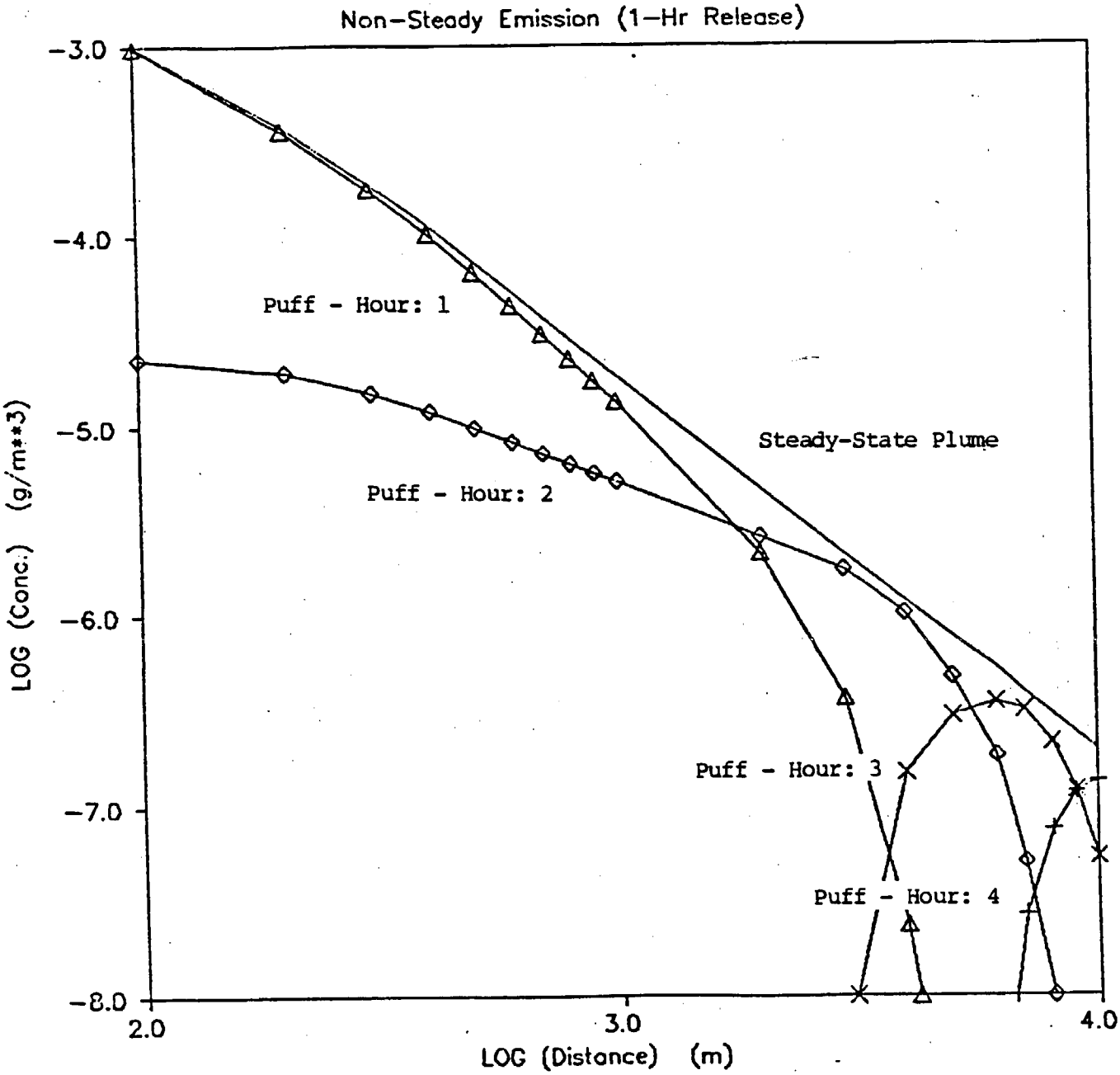

Figure 5.1-5. Concentration predictions of puff model #2 for non-steady emission conditions. Emission rate: 1 g/s, Emission duration: 1 hour, Wind speed: 1 m/s, Stability class: B, Stack height: 10 m, Mixing height: unlimited.

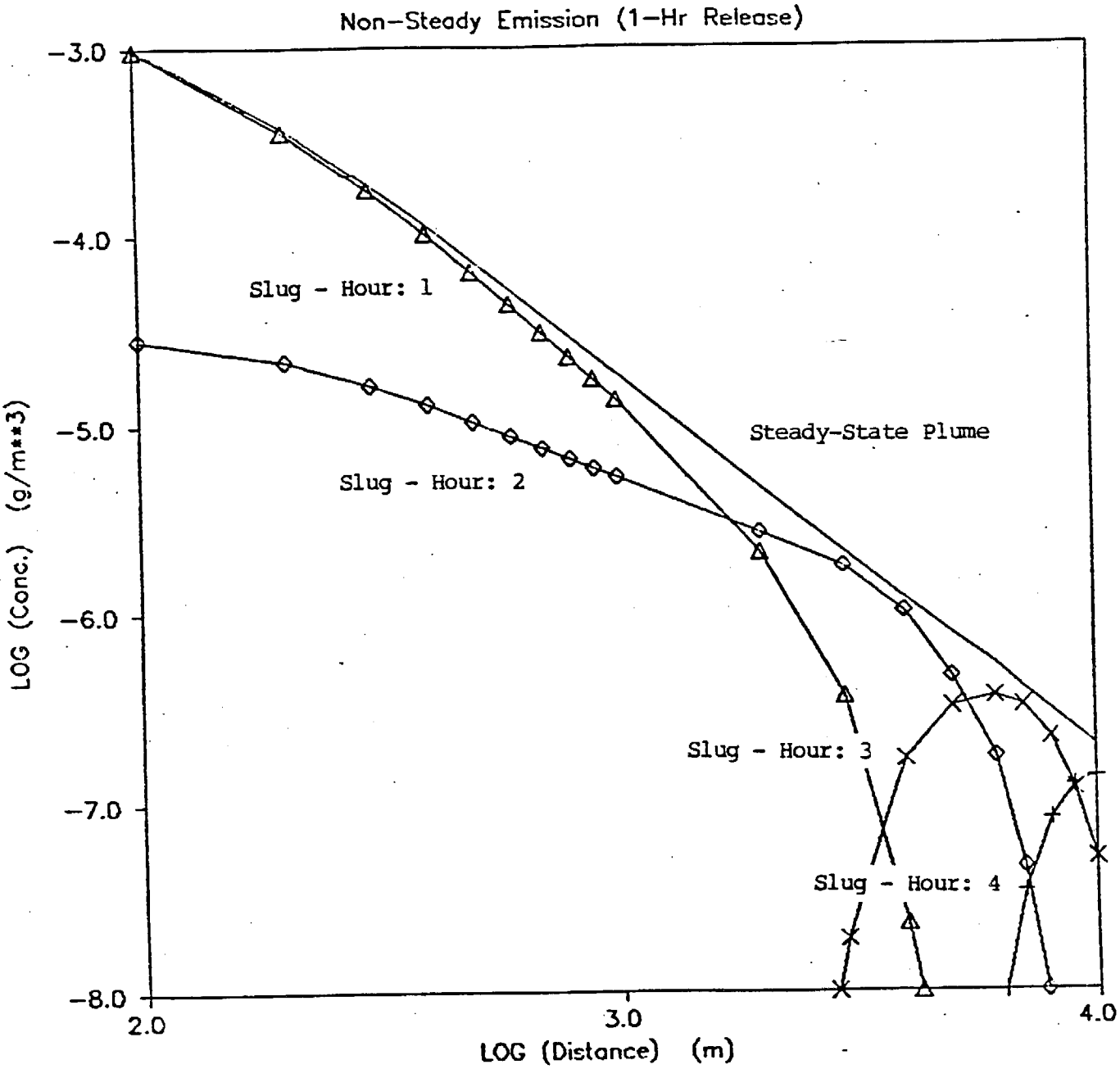

Figure 5.1-6. Concentration predictions of the slug model for non-steady emission conditions. Emission rate: 1 g/s, Emission duration: 1 hour, Wind speed: 1 m/s, Stability class: B, Stack height: 10 m, Mixing height: unlimited.

5.2 Dispersion Coefficients

A key modeling consideration is the specification of the horizontal and vertical Gaussian dispersion coefficients, s_y and s_z. The dispersion coefficients each consist of a number of different components:

$$s_y^2 = s_{yt}^2 + s_{yb}^2 + s_{yo}^2 + s_{ys}^2 \quad (5.2\text{-}1)$$

$$s_z^2 = s_{zt}^2 + s_{zb}^2 + s_{zo}^2 \quad (5.2\text{-}2)$$

where s_y, s_z are the total horizontal and vertical dispersion coefficients,
s_{yt}, s_{zt} are the components (m) of s_y and s_z due to atmospheric turbulence,
s_{yb}, s_{zb} are the components (m) of s_y and s_z due to plume buoyancy,
s_{yo}, s_{zo} are the initial values (m) of s_y and s_z due to the nature of the source (e.g., area source) or the rapid initial dilution associated with building downwash of point sources, and,
s_{ys} is the component of the horizontal dispersion coefficient (m) due to vertical wind shear effects.

ATMOSPHERIC TURBULENCE COMPONENTS

The basic strategy in the design of the dispersion module is to allow the use of the most refined data available in the calculation of s_{yt} and s_{zt} while providing for backup algorithms not requiring specialized data for situations in which these data are not available. Three levels of input data will be allowed:

(1) Direct turbulence intensity measurements,

(2) Estimates of the crosswind and vertical components of the wind direction fluctuation based on similarity theory and the micrometeorological scaling parameters u_*, w_*, L, and h, or,

(3) Pasquill-Gifford-Turner (PGT) dispersion coefficients.

The general forms of s_{yt} and s_{zt} (Hanna et al., 1977) for Options (1) and (2) are:

$$s_{yt} = s_v \; t \; f_y(t/t_{1y}) \quad (5.2\text{-}3)$$

$$s_{zt} = s_w \; t \; f_z(t/t_{1z}) \quad (5.2\text{-}4)$$

the approaching/passing distribution. The puff model lumps the pollutant mass into n packets (puffs), each with 1/n of the total emission (n = 100 in this test). The mass actually release from time t=0 to t=dt/n is packaged into the puff released at t=0. The puff lumping effect tends to result in a slightly premature arrival/departure of the pollutant, which is not seen in the case of steady emissions. In the non-steady runs, because the correct puff causality is obtained by increasing the puff release rate, the slug model is more computationally efficient.

In order to provide a cost-effective sampling scheme for a range of meteorological, emission, and source-receptor configurations, a hybrid circular puff/elongated slug scheme is proposed. The model will store information on the trailing endpoint of the emission cloud (required for the slug model) in addition to the data describing the leading edge (used in both the puff and slug models), at least initially, when the ratio $s_y/(u\ dt_e)$ is small. In the far-field, the initial elongation of the slug becomes unimportant, and puff sampling is nearly always the most efficient. For near-field receptors, however, if the emission rate changes rapidly, or a large wind direction change results in advection of a slug segment at a large angle to its long axis, the slug model may be more cost effective. Therefore, internal checks will be performed to a select the most appropriate sampling scheme. Although an all-slug or all-puff model could be engineered to produce appropriate results under all conditions, this hybrid approach, which takes advantage of the strengths of each algorithm, can produce the same results at lower computational cost.

where, s_v is the standard deviation (m/s) of the horizontal crosswind component of the wind,
s_w is the standard deviation (m/s) of the vertical component of the wind,
t is the travel time (s) of the plume to the receptor, and,
t_{ly}, t_{lz} are the horizontal and vertical Lagrangian time scales (s).

Equations (5.2-3) and (5.2-4) can be expressed in terms of the horizontal and vertical components (i_y and i_z) of the turbulence intensity using the following relationships.

$$i_y = s_v/u \simeq s_\theta \qquad (5.2\text{-}5)$$

$$i_z = s_w/u \simeq s_\phi \qquad (5.2\text{-}6)$$

where, u is the wind speed (m/s),
s_θ is the standard deviation (m/s) of the horizontal wind angle, and,
s_ϕ is the standard deviation (m/s) of the vertical wind angle.

The most desirable approach is to relate the dispersion coefficients directly to the measured turbulence intensity components (i_y and i_z). However, it is important that the quality of the observational data be considered in the selection of the method for computing the dispersion coefficients. For example, inaccurate observations of i_z, which is difficult to measure, may lead to less accurate modeling results that predictions based on more routine data. It is recommended that the default selection be Option 2, which uses similarity theory and micrometeorological variables derived from routinely available meteorological observations and surface characteristics.

Many laboratory experiments, field studies, and numerical simulations (e.g., Deardorff and Willis, 1975; Caughey, 1981; Lamb, 1981) have shown the importance and utility of convective scaling in the convective boundary layer. Convective scaling has been successfully applied to data collected at a wide variety of sites, including oceans, rural land surfaces (e.g., Hicks, 1985) and urban areas (Ching el al., 1983). Similarly, in the stable boundary layer, local scaling has been shown to apply (e.g., Hunt, 1982; Nieuwstadt, 1984). The micrometeorological model, (see Section 4) explicitly relates the aerodynamic and thermal characteristics of the surface to the sensible heat flux and momentum transfer rates that are used in the computation of the dispersion coefficients.

Weil (1985) and Briggs (1985) provide reviews on the use of similarity theory in diffusion models. In the convective boundary layer, Weil describes the turbulence characteristics in three layers:

Hanna et al. (1986) suggest that $C_v \simeq 1.6$. C_w has a value $\simeq 1.3$ (Nieuwstadt, 1984). The local friction velocity, u_{*1}, can be expressed (Nieuwstadt, 1984) as:

$$u_{*1} = u_* (1 - z/h)^{3/4} \qquad (5.2\text{-}15)$$

The modeling requires a formulation that yields the proper values and vertical variations for s_v and s_w in the convective, neutral, and stable limits, and one that provides a mechanism for interpolating the results for intermediate conditions without physically unrealistic discontinuities. The following equations for the neutral-convective boundary layer are based on the data discussed above and satisfy these conditions. The formulation for the entrainment layer is based on data reported by Caughey (1982).

Surface Layer: $z \leq 0.1\ h$ $\quad (L \leq 0)$

$$s_v = [4\ u_*^2\ a_n^2 + 0.35\ w_*^2]^{1/2} \qquad (5.2\text{-}18)$$

$$s_w = [1.6\ u_*^2\ a_n^2 + 2.9\ u_*^2\ (-z/L)^{2/3}]^{1/2} \qquad (5.2\text{-}19)$$

$$a_n = \exp[-0.9(z/h)] \qquad (5.2\text{-}20)$$

Mixed-Layer: $z = 0.1\text{-}0.8\ h$ $\quad (L \leq 0)$

$$s_v = [4\ u_*^2\ a_n^2 + 0.35\ w_*^2]^{1/2} \qquad (5.2\text{-}21)$$

$$s_w = [1.15\ u_*^2\ a_n^2 + 0.35\ w_*^2]^{1/2} \qquad (5.2\text{-}22)$$

Entrainment Layer: $z > 0.8\ h$ $\quad (L \leq 0)$

$$s_v = [4\ u_*^2\ a_n^2 + 0.35\ w_*^2]^{1/2} \qquad (5.2\text{-}23)$$

for $z = 0.8$ to $1.0\ h$

$$s_w = [1.15\ u_*^2\ a_n^2 + a_{c1}\ 0.35\ w_*^2]^{1/2} \qquad (5.2\text{-}24)$$

$$a_{c1} = [1/2 + (h-z)/(0.4h)] \qquad (5.2\text{-}25)$$

for $z = 1.0$ to $1.2\ h$

$$s_w = [1.15\ u_*^2\ a_n^2 + a_{c2}\ 0.35\ w_*^2]^{1/2} \qquad (5.2\text{-}26)$$

$$a_{c2} = [1/3 + (1.2h-z)/(1.2h)] \qquad (5.2\text{-}27)$$

Table 5.2-1

Comparison of Panofsky et al. (1977)/Hicks (1985)
s_v, s_w Formulations with Equations 5.2-(18-27)

Panofsky et al. data	Observed s_v vs. Panofsky	Observed s_v vs. Eqns. 5.2-(18-27)	Panofsky s_v vs. Eqns. 5.2-(18-27)
Average	(1.14, 1.20)	(1.14, 1.21)	(1.20, 1.21)
Corr. Coef.	.81	.84	.992
Average Bias	.07	.07	.00
Average Abs. Error	.10	.09	.02
RMSE	.13	.12	.02

Hicks 1985 data	Observed s_v vs. Hicks	Observed s_v vs. Eqns. 5.2-(18-27)	Hicks s_v vs. Eqns. 5.2-(18-27)
Average	(1.17, 1.12)	(1.17, 1.06)	(1.12, 1.06)
Corr. Coef.	.79	.77	.998
Average Bias	-.05	-.11	.06
Average Abs. Error	.20	.23	.06
RMSE	.27	.30	.08

Hicks 1985 data	Observed s_w vs. Hicks	Observed s_w vs. Eqns. 5.2-(18-27)	Hicks s_w vs. Eqns. 5.2-(18-27)
Average	(.98, 1.01)	(.98, .98)	(1.01, .98)
Corr. Coef.	.91	.91	.998
Average Bias	.03	.00	-.03
Average Abs. Error	.12	.11	.03
RMSE	.15	.14	.04

can be visualized as consisting of two steps: (1) distortion of the plume by changes in the wind direction or speed with height, followed by (2) vertical mixing of the distorted plume. Through the vertical mixing process, the vertical shear enhances the lateral spread of the plume. Pasquill (1976) suggests that the crosswind spread of the plume at large downwind distances (e.g., > 20 km) can be roughly approximated as ~0.75 x $d\theta$, where x is the downwind distance (m), and $d\theta$ is the change in the wind direction (radians) over the entire depth of the plume. The shear-induced crosswind spread is converted to an effective standard deviation, s_{ys}, by the Gaussian relationship 2.15 s_{ys} = (crosswind spread half-width), or:

$$s_{ys}^2 = 0.03 \ (x \ d\theta)^2 \qquad (5.2\text{-}38)$$

Eqn. (5.2-38) is not appropriate in regions of very large wind direction shear, (e.g., $d\theta \pm 180^o$ as in land/sea breeze circulations). An option to allow splitting and differential advection of puffs with $d\theta$ exceeding a critical value will be tested for inclusion in the model.

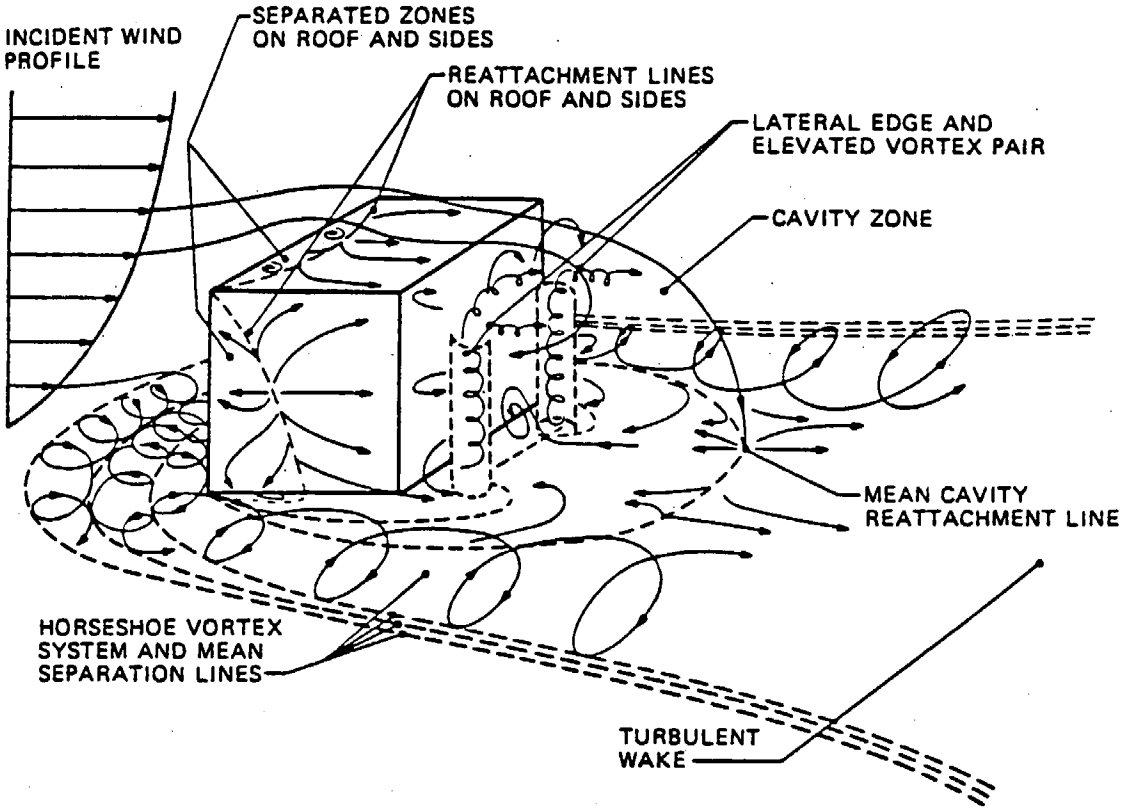

Figure 5.3-1. Flow near a sharp-edged building in a deep boundary layer. [From Hosker, (1984)].

As in ISC, an option will be provided to use H_w instead of H_b in Eqn. (5.3-4) to account for building edge effects for squat buildings with $H_w/H_b \leq 5$. For tall buildings, the maximum initial dispersion coefficients are:

$$s_{zo}(\max) = (2)^{-1/2} H_w \tag{5.3-5}$$

$$s_{yo}(\max) = 0.5\ (2)^{-1/2} H_w \tag{5.3-6}$$

The actual initial dispersion coefficients are computed as a linear function of the effective plume height:

$$s_{zo} = A_z\ s_{zo}(\max) \tag{5.3-7}$$

$$s_{yo} = A_y\ s_{yo}(\max) \tag{5.3-8}$$

where, for squat buildings,

$$A_z = \begin{cases} 0 & H_e \geq 3\ H_b \\ 1 - (H_e - H_b)/(2H_b) & H_b < H_e < 3\ H_b \\ 1 & H_e \leq H_b \end{cases} \tag{5.3-9}$$

for tall buildings,

$$A_z = \begin{cases} 0 & H_e \geq H_b + 2\ H_w \\ 1 - (H_e - H_b)/(2H_w) & H_b < H_e < H_b + 2\ H_w \\ 1 & H_e \leq H_b \end{cases} \tag{5.3-10}$$

and,

$$A_y = \begin{cases} 0 & H_e \geq 1.2\ H_b \\ 1 - (H_e - H_b)/(0.2H_b) & H_b < H_e < 1.2\ H_b \\ 1 & H_e \leq H_b \end{cases} \tag{5.3-11}$$

The maximum enhancement of the dispersion coefficients occurs for effective

5.4 Plume Rise

The plume rise relationships in the puff model are generalized to apply to a variety of source types and plume characteristics. It is proposed that the effects of the following be included in the plume rise algorithm:

- Plume buoyancy and momentum
- Stable atmospheric stratification
- Partial penetration of the plume into an elevated stable inversion layer
- Building downwash and stack-tip downwash effects
- Vertical wind shear

BASIC PLUME RISE EQUATIONS

The basic point source plume rise relationships are based on the Briggs (1975) equations. The plume rise due to buoyancy and momentum during neutral or unstable conditions, z_n, is:

$$z_n = [3F_m x/(\beta_j^2 u_s^2) + 3Fx^2/(2\beta_1^2 u_s^3)]^{1/3} \quad (5.4\text{-}1)$$

where F_m is the momentum flux (m^4/s^2),
F is the buoyancy flux (m^4/s^3),
u_s is the stack height wind speed (m/s),
x is the downwind distance (m),
β_1 is the neutral entrainment parameter ($\bar{}0.6$),
β_j is the jet entrainment coefficient ($1/3 + u_s/w$), and,
w is the stack gas exit speed (m/s).

The distance to final plume rise, x_f, is:

$$x_f = \begin{cases} 3.5\ x^* & F > 0 \quad (5.4\text{-}2) \\ 4D\ (w + 3u_s)^2/(u_s w) & F = 0 \quad (5.4\text{-}3) \end{cases}$$

$$x^* = \begin{cases} 14\ F^{5/8} & F \leq 55\ m^4/s^3 \quad (5.4\text{-}4) \\ 34\ F^{2/5} & F > 55\ m^4/s^3 \quad (5.4\text{-}5) \end{cases}$$

where D is the stack diameter (m).

If the stack height exceeds the mixed-layer height, then the stable plume rise equations (5.4-6) and (5.4-7) are used to compute the plume rise.

STACK-TIP DOWNWASH

If the ratio of the stack gas exit speed to the ambient wind speed is less than 1.5, the plume may be drawn into the lee of the stack. Briggs (1973) suggests modifying the stack height to adjust for this stack-tip effect:

$$h_s' = \begin{cases} h_s + 2D(w/u_s - 1.5) & w/u_s < 1.5 \quad (5.4\text{-}12) \\ h_s & w/u_s \geq 1.5 \quad (5.4\text{-}13) \end{cases}$$

BUILDING DOWNWASH

Wind tunnel observations of plume dispersion and plume rise indicate that plume rise can be significantly reduced by building downwash. Huber and Snyder (1982) found that during downwash conditions, plume rise was reduced by one-third below the value obtained in the absence of the building. In an analysis of plume rise observations, Rittmann (1982) found lower plume rise than predicted by the 2/3 law (a form of Eqn. 5.4-1) for smaller sources which are most likely to be affected by downwash. Several studies (e.g., Bowers and Anderson, 1981; Scire and Schulman, 1981; Thuillier, 1982) have shown that the ISC building downwash algorithm, which does not include the effects of building downwash on plume rise, may significantly underestimate concentrations during downwash conditions.

The increased mechanical turbulence in the building wake which leads to enhanced plume dispersion, causes a rapid dilution of the plume. This dilution reduces the rate of rise of the plume and leads to lower plume heights. One method of treating the initially high dilution rate is to assume an initial "dilution radius" for the plume (Scire and Schulman, 1979). This technique is incorporated in the Buoyant Line and Point Source (BLP) model (Schulman and Scire, 1980) and a modified version of the ISC model (Schulman and Hanna, 1986), and has been shown to produce more realistic estimates of ground-level concentrations during building downwash conditions.

The plume rise of a downwashed plume with $s_{yo} \leq s_{zo}$ during neutral-unstable conditions is given by:

$$z_d^3 + (3R_o z_d/\beta_1 + 3R_o^2/\beta_1^2)\, z_d = [3F_m x/(\beta_j^2 u_s^2) + 3Fx^2/(2\beta_1^2 u_s^3)] \quad (5.4\text{-}14)$$

where R_o is the dilution radius [$R_o = (2)^{1/2} s_{zo}$]. The factor of $(2)^{1/2}$

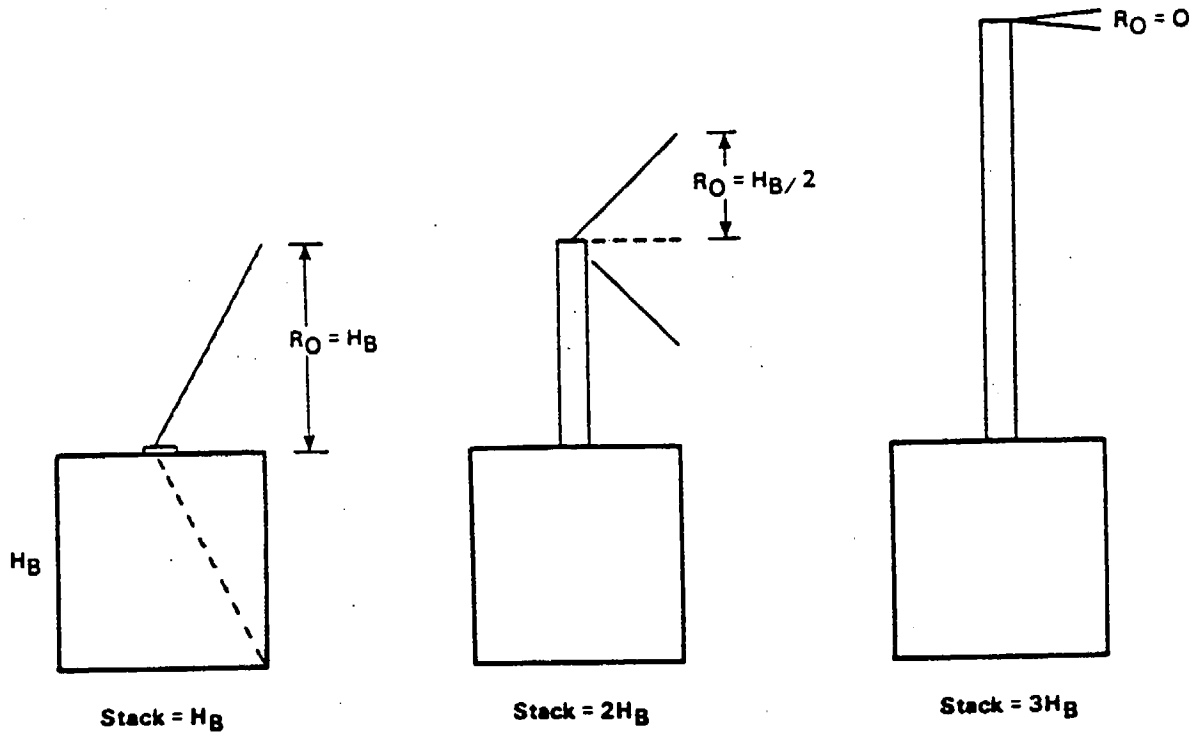

Figure 5.4-1. Illustration of the initial dilution radius, R_o, as a function of stack height for a squat building. [From Schulman and Scire (1981)]. Momentum plume rise is neglected in the figure.

5.5 Overwater and Coastal Dispersion

There are important differences in the structures of the marine and continental boundary layers which can have significant effects on plume dispersion in the overwater and coastal environments. These differences arise for three basic reasons (LeMone, 1978):

- Water has a high heat capacity and is partially transparent to solar radiation, resulting in a relatively small diurnal temperature range (~0.5 deg. C).
- The sea surface is generally more uniform and less aerodynamically rough than typical land surfaces.
- There is a constant source of moisture in the marine boundary layer.

As a result of these differences, the sensible heat flux over the open water is typically more than an order of magnitude less than over land. The absence of a strong sensible heat flux to drive the marine mixed-layer and the small surface roughness result in relatively low mixing heights that offer the potential for significant plume trapping effects. LeMone (1978) indicates that the typical marine mixing depth is only about 500 m. Data from three offshore and coastal experiments reported by Hanna et al. (1985) (two of which were conducted in California) show many hours with mixing heights less than 100 m.

Another result is that the diurnal and annual variations of stability over water are completely unrelated to the typical overland behavior. For example, North Sea observations of water and air temperatures reported by Nieuwstadt (1977) (Figure 5.5-1) show that temperature inversions typically persist most of the day in June, while unstable conditions occur all day in January. During other times of the year, the overwater diurnal stability cycle is out of phase with the overland cycle (i.e., stable over water during the day and unstable at night).

Techniques for determining overwater mixing height, stability, and turbulence levels based on the air-sea temperature difference, wind speed, and the specific humidity have been discussed in Section 4.2. These methods will be applied to the portions of the grid over water. At the land-sea interface, rapid changes in the dispersion characteristics may occur which can significantly affect the ground-level concentrations from coastal sources. The puff model formulation is well-suited to accomodate these spatial changes in the coastal transition zone.

A typical situation during stable onshore flow conditions is shown in Figure 5.5-2. A narrow plume imbedded in the stable layer above the shallow mixed-layer is intercepted by a growing Thermal Internal Boundary Layer (TIBL). The growth of the TIBL is caused by the sensible heat flux associated with solar heating of the land surface. The convective overland conditions can

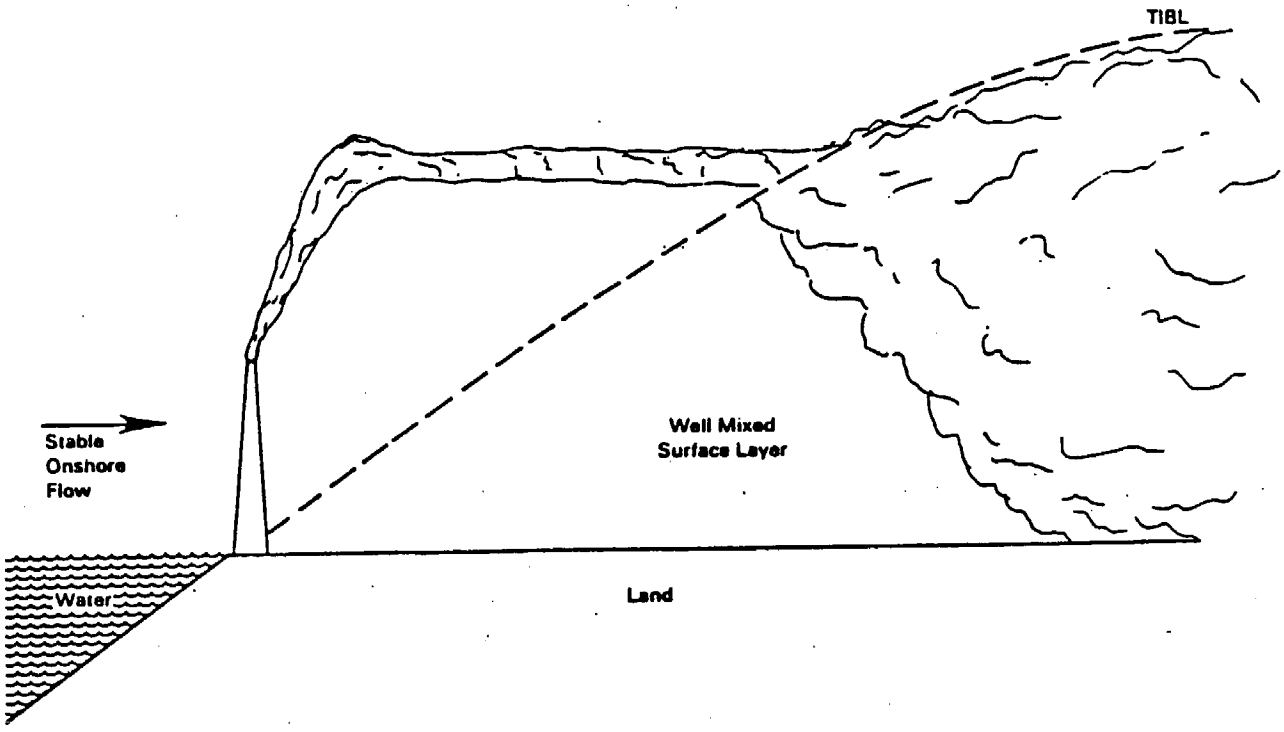

Figure 5.2-2. Schematic illustration of a typical coastal fumigation condition. [From Hanna et al. (1985)].

The empirical relationships (5.5-1) and (5.5-2) are based on observational data from Raynor et al. (1979), Kerman (1982), and Stunder and Sethuraman (1985). With Option 1, subgrid scale land use data is used for a more detailed specification of coastal features (islands, inlets, etc.). Figure 5.5-3 illustrates the subgrid scale representation of the land-sea boundary.

If the second option is selected, the turbulence and dispersion characteristics over water are computed in the same way as with Option 1. However, the detailed TIBL height and plume interception calculations are replaced with a more approximate representation of the land-sea boundary. The transition from marine to continental disperson rates is assumed to occur at the coastal boundary determined from the land use data at the computational grid points only (e.g., in Figure 5.5-3, the land-sea boundary is assumed to be midway between a computational grid point with "L" and an adjacent point with "+"). In addition, the continental vertical mixing depth is determined by the overland mixed-layer height at the computational grid point rather than the x-dependent TIBL height. These approximations are likely to be adequate for many applications and will reduce the computational and input requirements of the model.

5.6 Complex Terrain

The model will respond to the presence of terrain on two scales. The effect of terrain that extends over a scale large enough to be resolved by the grid used in the flow field model will be manifest in the boundary conditions for the flow field. A puff embedded in this flow will either rise with the flow along the surface of the terrain, or it will be steered by the flow along the terrain, depending on the degree of stratification. Concentration estimates will be calculated along the trajectory of the puff as if the terrain beneath it were flat. Effects of terrain that are not resolved by the grid used in the flow field model will be treated in a separate subroutine, CTSG (COMPLEX TERRAIN ALGORITHM FOR SUB-GRID SCALE FEATURES).

CTSG accepts the flow field produced by the flow model (both the wind and temperature structure) in the vicinity of a terrain feature as the incident flow toward that feature. It then proceeds to simulate changes in the flow and in the rate of dispersion that are induced by that terrain feature. CTSG will require at a minimum the following attributes for each sub-grid scale terrain feature:

Center	: relative to the origin of the modeling grid
Orientation	: angle from North to the "long axis" of the hill
Aspect Ratios	: ratio of one half the length of each "axis",measured at one half the hill height, to the height of the hill
Height	: peak elevation above the mean local elevation of the underlying gridded terrain.

At the core of CTSG is the modeling approach adopted in CTDM, the complex terrain model being developed in EPA's Complex Terrain Model Development program. Several simplifications and extensions to CTDM are envisioned for CTSG. Our goal in designing CTSG is to produce a puff algorithm that contains those elements of the CTDM approach that have the greatest impact on ground-level concentrations. This will require a framework similar to that in CTDM, and will allow a more elaborate version of CTSG to be prepared later in this program if the ARB wishes CTSG to be equivalent to the final version of CTDM (due in late 1987).

A central feature of CTDM adopted for use in CTSG is the dividing-streamline concept. The flow is taken to be composed of two layers. In the upper layer, the approach flow has sufficient energy to transport a fluid parcel up and over the hill against a stable potential density gradient. In the lower layer, the flow is constrained to travel around the hill. This concept was suggested by theoretical arguments of Drazin (1961) and Sheppard (1956) and was demonstrated through laboratory experiments by Riley et al. (1976), Brighton (1978), Hunt and Snyder (1980), Snyder (1980), and Snyder and Hunt (1984).

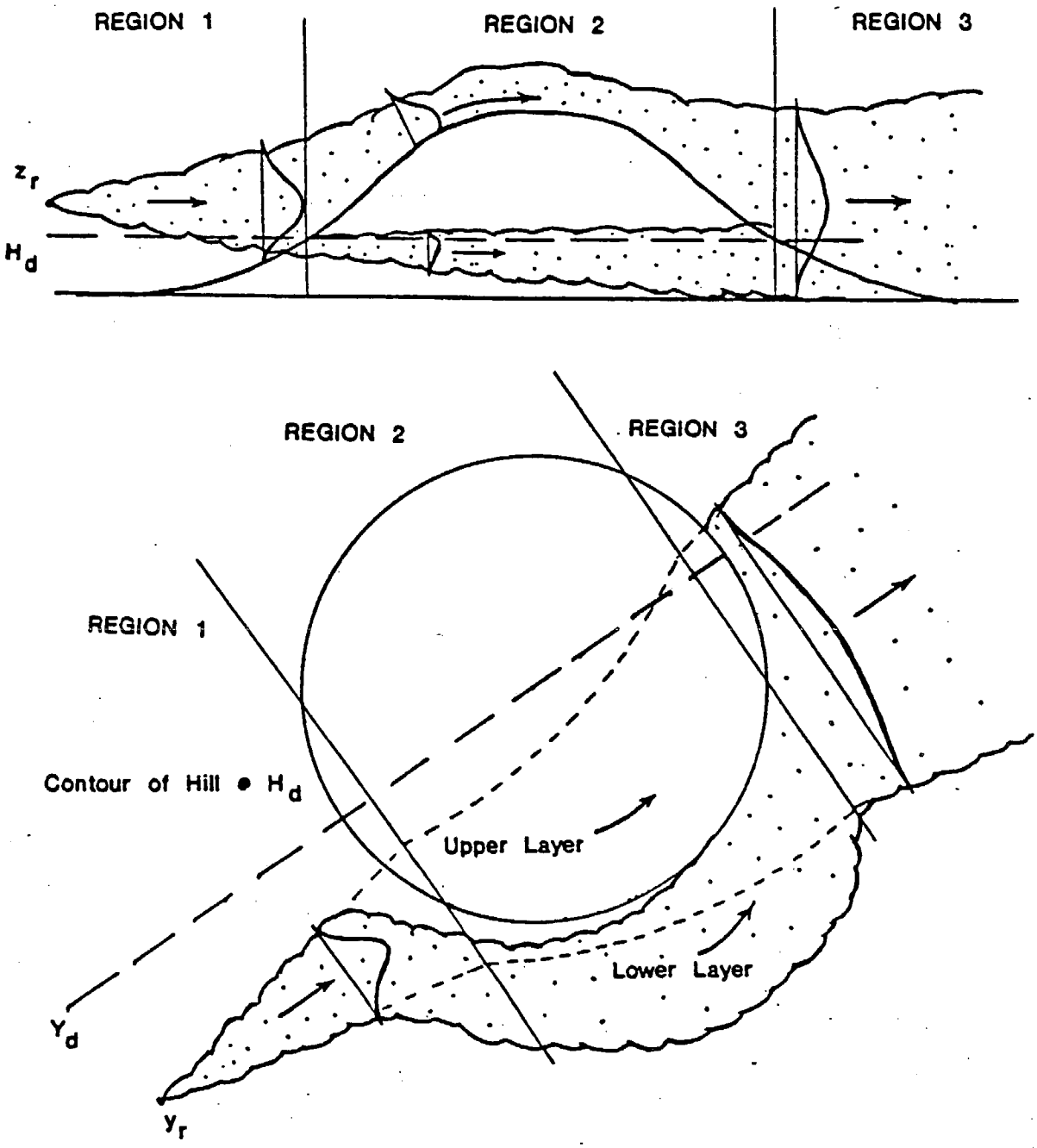

Figure 5.6-1. Illustration of the three distinct regions and the two layers in the vertical for modeling concentrations around a sub-grid scale terrain feature.

The subscript o denotes a value obtained at $t=t_o$ and the subscript * denotes

$$s_{x*}^2 = s_x^2(t_R) - s_x^2(t_o) \qquad \text{(for x = y or z)} \qquad (5.6\text{-}4)$$

Tz and Ty are factors that contain the effects of the distortion of the flow over the hill on the rates of vertical and lateral diffusion.

The distribution functions are given by

$$F_y = \exp(-.5\ [y_R/Tl - y_r]^2/s_{ye}^2)$$

$$F_z = \exp(-.5\ [z_r - H_d]^2/s_{ze}^2)\ \text{erfc}(s_{z*}\ [H_d - z_r]/[\ 2\ Tz\ s_{ze}\ s_{zo}]) \qquad (5.6\text{-}5)$$

$$+ \exp(-.5\ [z_r + H_d]^2/s_{ze}^2)\ \text{erfc}(s_{z*}\ [H_d + z_r]/[\ 2\ Tz\ s_{ze}\ s_{zo}])$$

where Tl is a measure of the lateral deformation in the flow. F_y contains information on the deflection in the trajectory over the hill as well as information on changes in the diffusivity. The lateral offset of the receptor from the centerline of the plume is modified by the appearance of the lateral distortion factor Tl in the numerator of the exponential term, and the change in the diffusivity is contained in the effective lateral plume size, s_{ye}. F_z also contains the change in diffusivity in the effective vertical plume size, s_{ze}, and it includes complete reflection from the surface of the hill (marked by H_d) for only that material which lay above H_d at $t=t_o$. "Cutting" the plume at $z=H_d$ and allowing reflection from this surface gives rise to the combination of exponential and error function products in Equation 5.6-5. A full discussion of the development of these equations is contained in Strimaitis et al. (1984) and in DiCristofaro et al. (1985).

In the case of a puff, the sampling function allows us to rewrite the concentration estimate for a receptor on the surface (Equation 5.6-2) as

$$GLC = \frac{Q}{t_1 - t_2} \frac{F_y(t_R)\ F_z(t_R)}{4\pi u\ s_{ze}\ s_{ye}} \left\{ \text{erf}\left(\frac{t_2 - t_R}{\sqrt{2} s_{ye}/u} \right) - \text{erf}\left(\frac{t_1 - t_R}{\sqrt{2} s_{ye}/u} \right) \right\} \qquad (5.6\text{-}6)$$

where Q is now the total mass of material (g) in the puff.

These expressions do not include the effect of an elevated inversion on the vertical distribution of the puff. When a mixing lid is present, the F_z function contains many more terms to simulate multiple reflections. The derivation of F_z with a mixing lid is an extension not found in CTDM. For a mixing lid at z_L (m),

$$F_z(H_d=\emptyset, z_L=\infty) = 2\ \exp(-.5[z_r/s_{ze}]^2) \qquad (5.6\text{-}11)$$

which is the form commonly used for flat terrain.

As indicated in Equation 5.6-3, the factors Tz and Ty are important in specifying the effect of the hill on the rates of dispersion. The theory for a narrow plume embedded in a flow with axisymmetric strain was developed by Hunt and Mulhearn (1973), and their results indicate that that the following approximations may be made:

$$Tz^{-2} = Th^{-2}(t)\ S_z^{-2}(t) \int_{t_o}^{t} S_z^2(t')\ 2K_z(t')\ dt' \Big/ \int_{t_o}^{t} 2K_{oz}(t')\ dt'$$

$$Ty^{-2} = Tl^{-2}(t)\ S_y^{-2}(t) \int_{t_o}^{t} S_y^2(t')\ 2K_y(t')\ dt' \Big/ \int_{t_o}^{t} 2K_{oy}(t')\ dt' \qquad (5.6\text{-}12)$$

where the strain functions are given by

$$S_z(t) = \exp(1\text{-}Th(t)) \qquad S_y(t) = \exp(1\text{-}Tl(t)) \qquad (5.6\text{-}13)$$

and the deformation factors Th and Tl are scaled from potential flow calculations over the crest of an ellipsoid. The integrals in Equation 5.6-12 are evaluated numerically along the trajectory of the center of the puff. Vertical and lateral diffusivities (m^2/s) in the absence of the terrain are denoted by K_{oz} and K_{oy} whereas those that are influenced by the terrain are denoted by K_z and K_y. Each is found from the dispersion coefficients as

$$2K(t) = d(s^2)/dt \qquad (5.6\text{-}14)$$

where s denotes either s_y or s_z. The effect of the terrain on the diffusivity is assumed to be restricted to the change in the vertical turbulence over the hill. We write the dispersion coefficient as the product of the turbulence and a function of time (in the absence of terrain). Over the hill, the vertical turbulence velocity is assumed to increase with wind speed as in the "inner layer" theory, and the lateral turbulence velocity is assumed constant as in the "rapid distortion" theory (e.g. see Britter et al. (1981) for a discussion of these theories). These assumptions tend to accentuate the effect of the hill in the diffusion calculation.

its argument into account) is positive when both the receptor and the plume centerline lie on the same side of Y_d. If all of the material were to reside on one side of Y_d at t_o, then F_y would equal either 0 or 2, depending on whether the receptor were on the other side or on the same side of Y_d.

F_z contains information about the amount of material below H_d at t_o, and about how this material is sampled in the vertical. The form is a product of an exponential function and error functions in which the sampling height z_R is most evident in the exponential function, and the effects of splitting the plume at H_d is contained in the error functions. A full discussion of the development of these equations is contained in Strimaitis et al. (1984) and in DiCristofaro et al. (1985).

In the case of a puff, the sampling function allows us to rewrite the concentration estimate for a receptor on the surface (Equation 5.6-15) as

$$GLC = \frac{Q}{t_1 - t_2} \frac{F_y(t_R)\ F_z(t_R)}{4\pi u\ s_z\ s_y} \left\{ \operatorname{erf}\left(\frac{t_2 - t_R}{\sqrt{2} s_y / u}\right) - \operatorname{erf}\left(\frac{t_1 - t_R}{\sqrt{2} s_y / u}\right) \right\} \qquad (5.6\text{-}18)$$

where Q is the total mass of material (g) in the puff.

These expressions do not include the effect of an elevated inversion on the vertical distribution of the puff. When a mixing lid is present, the F_z function contains many more terms to simulate multiple reflections. This has been derived, and the result is similar to that discussed in 5.6.1. However, the presence of a lid to the growth of s_z would only affect dispersion below H_d in the rare (we think) case of z_L slightly greater than H_d, so we have no plans at the present time for including z_L in the formulation for dispersion in the lower layer.

Table 5.7-1

Factors Influencing Dry Deposition Rates

Micrometeorological Variables	Depositing Material	Surface Variables
Aerodynamic roughness	Particles	Accommodation
- Mass transfer		- Exudates
(a) Particles	Agglomeration	- Trichomes
(b) Gases	Diameter	- Pubescence
- Heat	Density	- Wax
- Momentum	Diffusion	Biotic surfaces
Atmospheric stability	- Brownian	Canopy growth:
Diffusion, effect of:	- Eddy equal to	- Dormant
- Canopy	(a) Particle	- Expanding
- Diurnal variation	(b) Momentum	Senescent
- Fetch	(c) Heat	Canopy structure:
Flow separation:	- Effect of canopy on	- Areal density
- Above canopy	Diffusiophoresis	- Bark
- Below canopy	Electrostatic effects	- Bole
Friction velocity	- Attraction	- Leaves
Inversion layer	- Repulsion	- Porosity
Pollutant concentration	Gravitational settling	- Reproductive structure
Relative humidity	Hygroscopicity	- Soils
Seasonal variation	Impaction	- Stem
Solar radiation	Interception	- Type
Surface heating	Momentum	Electrostatic properties
Temperature	Physical properties	Leaf-vegetation:
Terrain	Resuspension	- Boundary layer
- Uniform	Shape	- Change at high winds
- Nonuniform	Size	- Flutter
Turbulence	Solubility	- Stomatal resistance
Wind velocity	Thermophoresis	Non-biotic surfaces
Zero-plane displacements		pH effects on:
- Mass transfer	Gases	- Reaction
(a) Particles		- Solubility
(b) Gases	Chemical activity	Pollutant penetration and distribution in canopy
- Heat	Diffusion:	Prior deposition loading
- Momentum	- Brownian	Water
	- Eddy	
	Partial pressure in equilibrium with surface	
	Solubility	

From: Sehmel (1980)

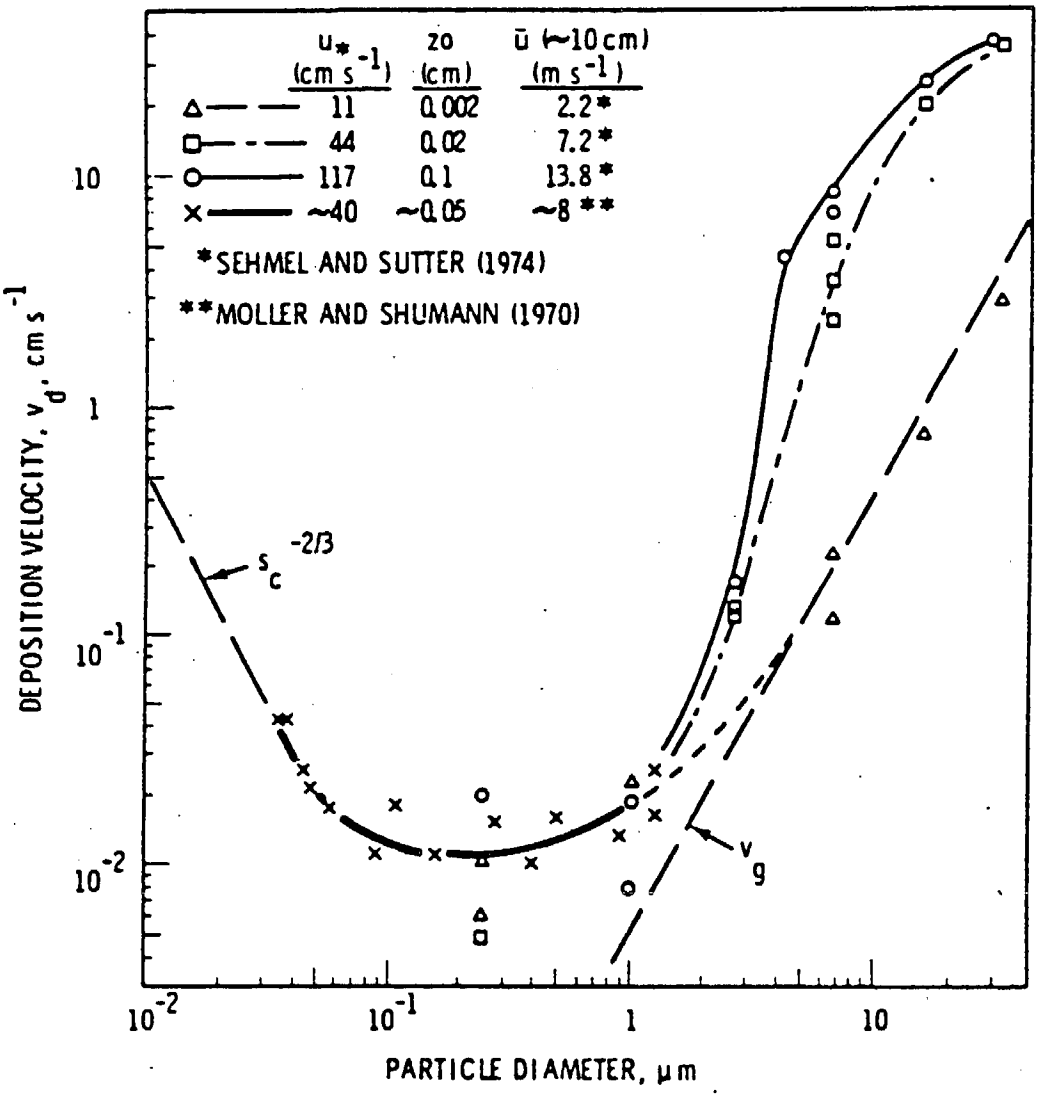

Figure 5.7-2. Observed deposition velocities as a function of particle size for 1.5 g/cm^3 density particles. Measured by Sehmel and Sutter (1974) and Moller and Schumann (1970). Figure from Slinn et al. (1978).

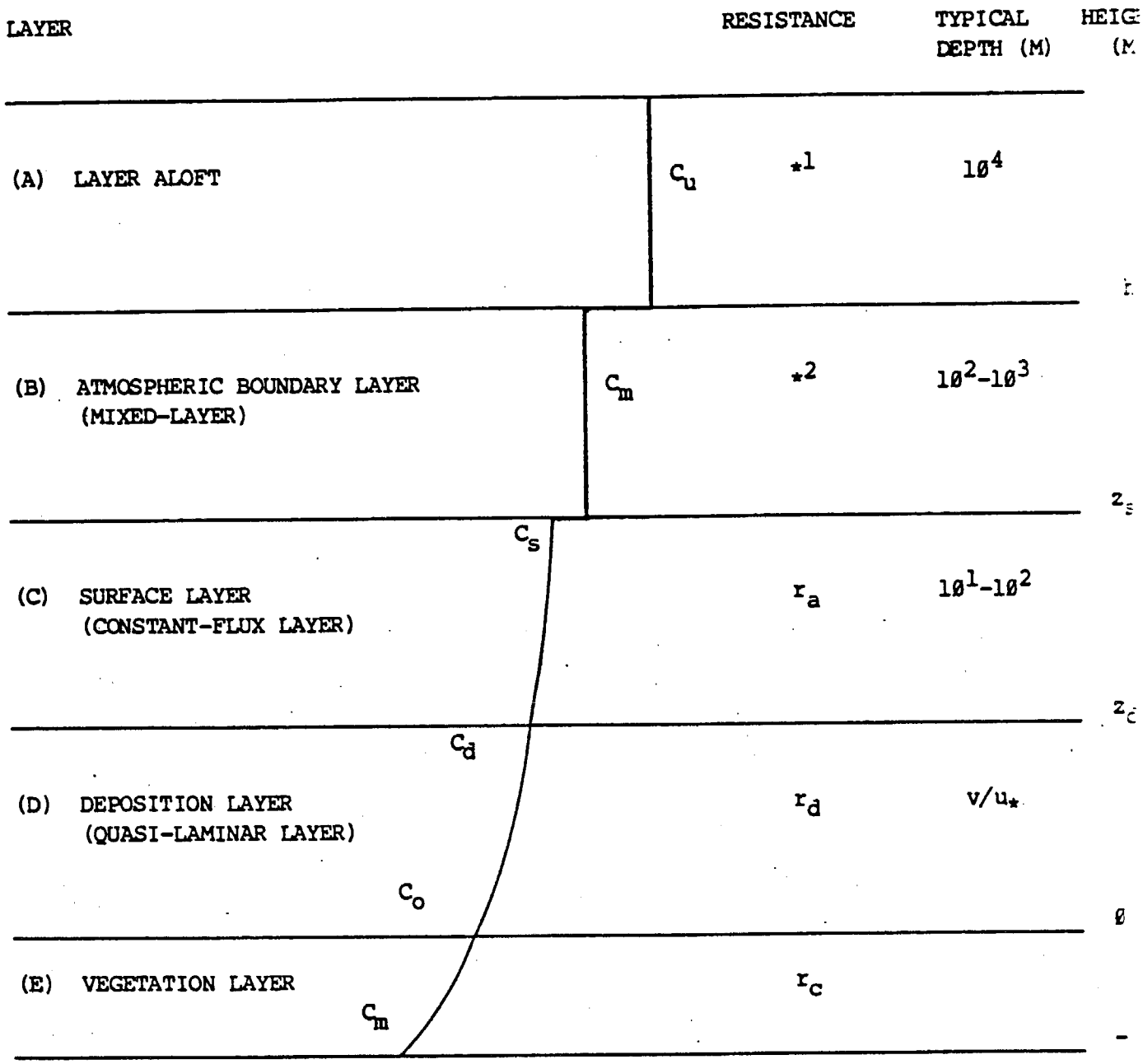

*1 Material in the top layer is not available for deposition at the surface until entrained into the mixed-layer.

*2 Overall mixed-layer resistance included in Eqn. (5.7-5).

Figure 5.7-3. Multilayer structure used in the dry deposition resistance model. (Adapted from Slinn et al., 1978).

D_{bl} during stable conditions (Brost and Wyngaard,1978) is:

$$D_{bl} = k_1 u_* h \qquad (5.7\text{-}3)$$

and during neutral or unstable conditions is:

$$D_{bl} = \text{Maximum } [k_1 u_* h \ , \ k_2 w_* h] \qquad (5.7\text{-}4)$$

where k_1 and k_2 are constants with default values of 0.01 and 0.1, respectively.

The term $v_d C_s$ can be written as $v_d' C_m$, where v_d' is an effective deposition velocity taking into account boundary layer mass transfer. From Eqn. (5.7-2), v_d' is:

$$v_d' = D_{bl} v_d / [D_{bl} + v_d (h - z_s)] \qquad (5.7\text{-}5)$$

When turbulent mixing within Layer B is rapid compared to the rate of deposition at the surface, the atmosphere quickly replaces material that is deposited. During these conditions, D_{bl} is large, and $v_d' \sim v_d$. However, the rate of deposition can be limited by the rate of pollutant transfer through Layer B to the vicinity of the surface. During stable conditions, D_{bl} may be small compared to $v_d(h-z_s)$, and v_d' may be substantially smaller than v_d. In the near-field of a source, before the plume has spread through the boundary layer, it is assumed that $v_d' \sim v_d$. This allows the near-field vertical Gaussian distribution to be maintained.

The resistances in the layers below the reference height in the surface constant-flux layer determine v_d. The parameterization of these resistances is discussed separately for gases and particles in Sections 5.7.1 and 5.7.2 below. Once v_d is determined, v_d' is computed from Eqn. (5.7-5). Each time step, the mass of the pollutant in the puff is adjusted to account for the dry removal:

$$Q_m(t+dt) = Q_m(t) \exp \left[-(v_d' dt/ds) \int_s^{s+ds} g(s')\, ds' \right] \qquad (5.7\text{-}6)$$

$v_d C_s = v_d' C_m$

From 5.7-2 $D_{bl}(C_m - C_s)/(h - z_s) = v_d C_s \Rightarrow v_d (h - z_s) = D_{bl}\left(\frac{C_m}{C_s} - 1\right)$

$D_{bl}(C_m - C_s)/(h - z_s) = v_d' C_m \Rightarrow v_d' (h - z_s) = D_{bl}\left(1 - \frac{C_s}{C_m}\right)$

} eliminate C_m/C_s and find 5.7-5

ϕ_H is a stability correction term, and,
L is the Monin-Obukhov length (m).

The stability correction term accounts for the effects of buoyancy on the eddy diffusivity of the pollutant. It is assumed that the pollutant transfer is similar to that for heat (Wesely and Hicks, 1977). The surface roughness length will be based on land use type or, if available, input as a gridded field. Over water, due to the effect of the wind on wave height, the surface roughness length varies. Hosker (1974) parameterizes z_o over water as:

$$z_o = 2.0 \times 10^{-6} u^{2.5} \qquad (5.7\text{-}10)$$

where u is the wind speed (m/s) at 10 m.

DEPOSITION LAYER RESISTANCE

Due to the importance of molecular diffusion to the transport through the laminar deposition layer, the deposition layer resistance for gaseous pollutants is parameterized in terms of the Schmidt number:

$$r_d = d_1 Sc^{d2}/(k u_*) \qquad (5.7\text{-}11)$$

where Sc is the Schmidt number (v/D),
D is the molecular diffusivity of the pollutant (m^2/s), and,
d_1, d_2 are empirical parameters.

Experimental studies summarized by Hicks (1982) suggest a range of values for the empirical variables of 1.6 to 16.7 for d_1 and 0.4 to 0.8 for d_2. Intermediate values of d1 = 5, and d2 = 2/3 are recommended based on Shepard (1974), Slinn et al. (1978), and Hicks (1982).

CANOPY RESISTANCE

The canopy resistance is the resistance for gases in the vegetation layer. There are three main pathways for uptake/reaction of the pollutant within the vegetation or surface:

(1) Transfer through the stomatal pore and dissolution or reaction in the mesophyll cells.

(2) Reaction with or transfer through the leaf cuticle.

(3) Transfer into the ground/water surface.

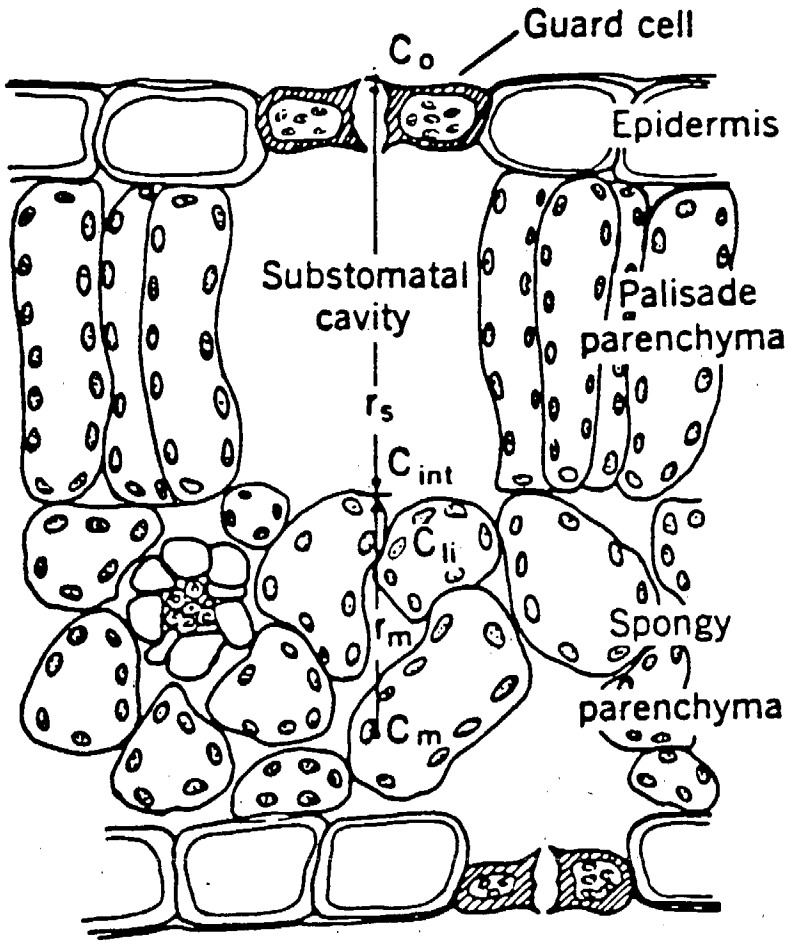

Figure 5.7-4. Schematic cross-section of a leaf illustrating the internal foliage resistance to pollutant transfer through the stomatal pore, substomatal cavity, and into the mesophyll (spongy parenchyma) cells. [From O'Dell et al., (1977)].

$$r_{cut} = (A_{SO2}/A)\ r_{cut}(SO_2) \qquad (5.7\text{-}16)$$

where A is the reactivity parameter for the depositing gas,
A_{SO2} is the reactivity of SO_2 (~8.0), and,
$r_{cut}(SO_2)$ is the empirically determined cuticle resistance (s/m) of SO_2.

Pleim et al. (1985) suggest $r_{cut}(SO_2)$ is ~17 s/cm. Reactivity values for other pollutants are estimated at 8.0 (NO_2), 15.0 (O_3), 18.0 (HNO_3), and 4.0 (PAN).

GROUND/WATER RESISTANCE

The third pathway through the "vegetation layer" does not involve vegetation at all. It is deposition directly to the ground or water surface. In moderately or heavily vegetated areas, the internal foliage and cuticle resistances usually control the total canopy resistance. However, in sparsely vegetated area of California, deposition directly to the surface may be an important pathway. Over water, deposition of soluble pollutants can be quite rapid.

The ground resistance, r_g, over land surfaces can be expressed (Pleim et al., 1985) relative to a reference value for SO_2:

$$r_g = (A_{SO2}/A)\ r_g(SO_2) \qquad (5.7\text{-}17)$$

where $r_g(SO2)$ is the ground resistance of SO_2 (~5 s/cm).

Slinn et al. (1978) parameterize the liquid phase resistance of the depositing pollutant as a function of its solubility and reactivity characteristics. Their results can be expressed as:

$$r_g = H/(\alpha_* d_3 u_*) \qquad (5.7\text{-}18)$$

where H is the Henry's law constant (ratio of gas to liquid phase concentration of the pollutant),
α_* is a solubility enhancement factor due to the aqueous phase reactivity of the pollutant (α_* ~10^3 for SO_2, ~1 for CO_2), and,
d_3 is a constant (~4.8×10^{-4}).

measure of the likelihood of impaction of the particle. It increases with increasing particle size.

The gravitational settling velocity is a function of the particle size, shape, and density. For spheres, the settling velocity is given by the Stokes equation:

$$v_g = [(d_p)^2 \, g \, (P_p - P_g) \, C]/(18 \, v) \qquad (5.7\text{-}21)$$

where d_p is the particle diameter (m),
P_p is the particle density (g/m^3),
P_g is the air density (g/m^3), and,
C is the Cunningham correction for small particles. This correction given by:

$$C = 1 + (2 \lambda / d_p)[a_1 + a_2 \, \mathrm{Exp}(-a_3 \, d_p/\lambda)] \qquad (5.7\text{-}22)$$

where λ is the mean free path of air molecules (6.53×10^{-6} cm), and
a_1, a_2, a_3 are constants (1.257, 0.40, 0.55, respectively).

Because of the sensitivity of the particle deposition velocity to particle size, v_d will be computed for each of a number of size categories (e.g., up to 20 or more). The effective deposition velocity will be determined based on a weighting of the individual deposition velocities composing the distribution. The size categories and the mass distribution will be user-specified inputs to the model.

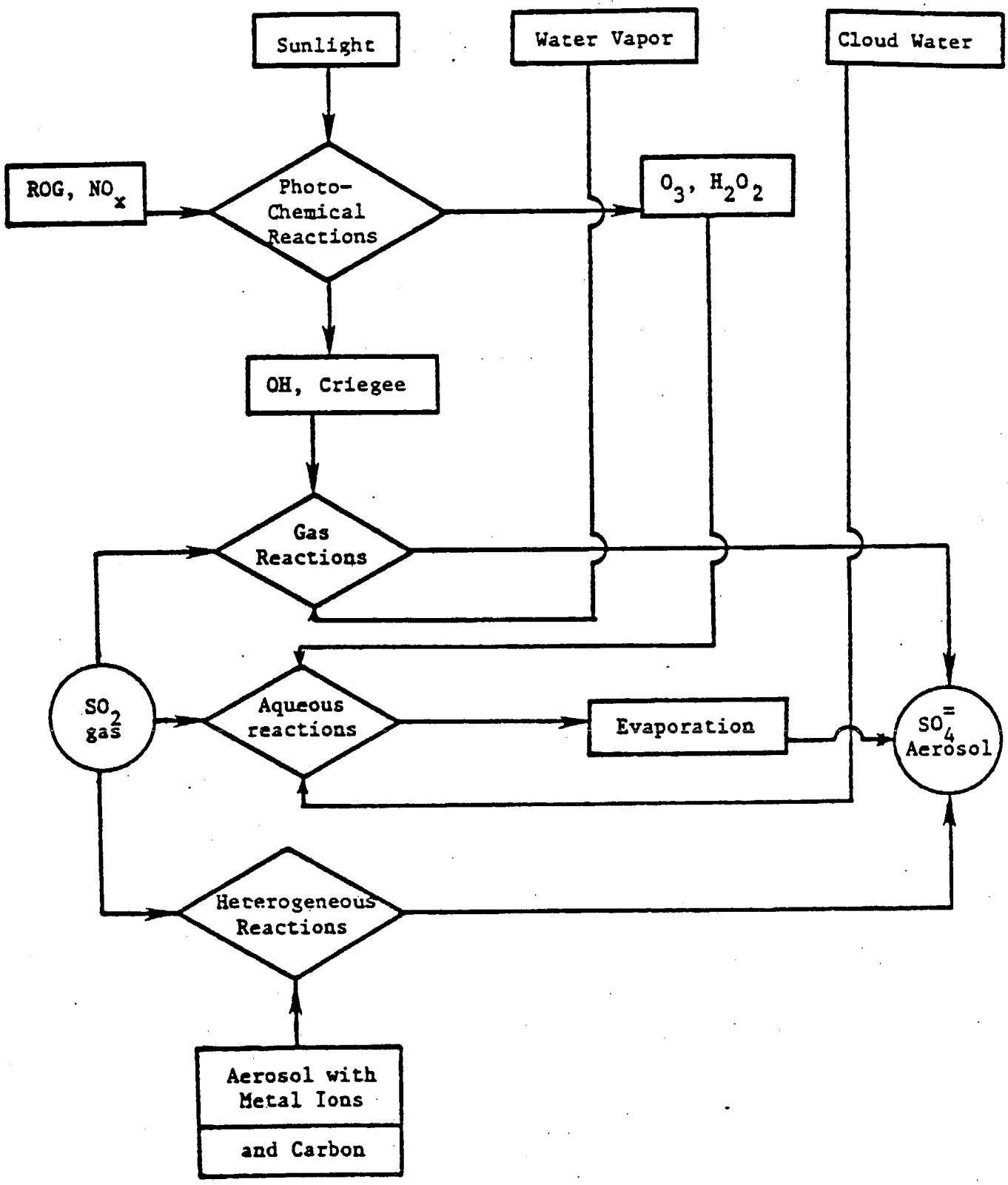

Figure 5.8-1. SO_2 oxidation pathways. [From Scire et al., (1984)].

process is reversible. Equilibrium is established between nitric acid, ammonia, and ammonium nitrate:

$$NH_4NO_3 \text{ <---> } HNO_3(g) + NH_3(g) \qquad (5.8\text{-}1)$$

The equilibrium constant for this reaction ($K = [NH_3][HNO_3]/[NH_4NO_3]$) is a nonlinear function of temperature and relative humidity as shown in Figure 5.8-3 (Stelson and Seinfeld, 1982). The equilibrium constant can vary several orders of magnitude over a typical diurnal cycle. Given fixed amounts of total nitrate, ammonia, and water vapor, higher NH_4NO_3 concentrations are expected at night due to lower nighttime temperatures and higher relative humidities. Thus, the nitrate aerosol cannot be considered a stable product like sulfate. Also, unlike sulfate, the ambient concentration of nitrate is limited by the availability of ammonia which is preferentially scavenged by sulfate (Stelson et al., 1983).

The transformation pathways for the five active pollutants (SO_2, SO_4, NO_x, HNO_3, and NO_3) included in the MESOPUFF II scheme are shown in Figure 5.8-4. Transformation rate expressions were developed by statistically analyzing hourly transformation rates produced by a photochemical model. The photochemical model employed the $RHC/NO_x/SO_x$ chemical mechanism of Atkinson et al. (1982). Plume SO_x/NO_x dispersing into background air containing ozone and reactive hydrocarbons was simulated over a wide range of conditions representing different solar radiation intensities, temperatures, dispersion conditions, background ozone and RHC concentrations, plume NO_x concentrations and emission times. The following transformation rate expressions, representing curve fits to the daytime hourly conversion rates predicted by the photochemical model, were determined:

$$k_1 = 36\ R^{\emptyset.55}[O_3]^{\emptyset.71}S^{-1.29} + k_{1aq} \qquad (5.8\text{-}2)$$

$$k_2 = 1206\ [O_3]^{1.5}\ S^{-1.41}\ [NO_x]^{-\emptyset.33} \qquad (5.8\text{-}3)$$

$$k_3 = 1261\ [O_3]^{1.45}\ S^{-1.34}\ [NO_x]^{-\emptyset.12} \qquad (5.8\text{-}4)$$

where k_1 is the SO_2 to SO_4 transformation rate (percent/hour),
k_2 is the NO_x to $HNO_3 + RNO_3$ transformation rate (percent/hour),
k_3 is the NO_x to HNO_3 (only) transformation rate (percent/hour),
R is the total solar radiation intensity (kw/m^2),
S is a stability index ranging from 2 to 6 (PGT class A and B-2, C=3, D=4, E=5, F=6),

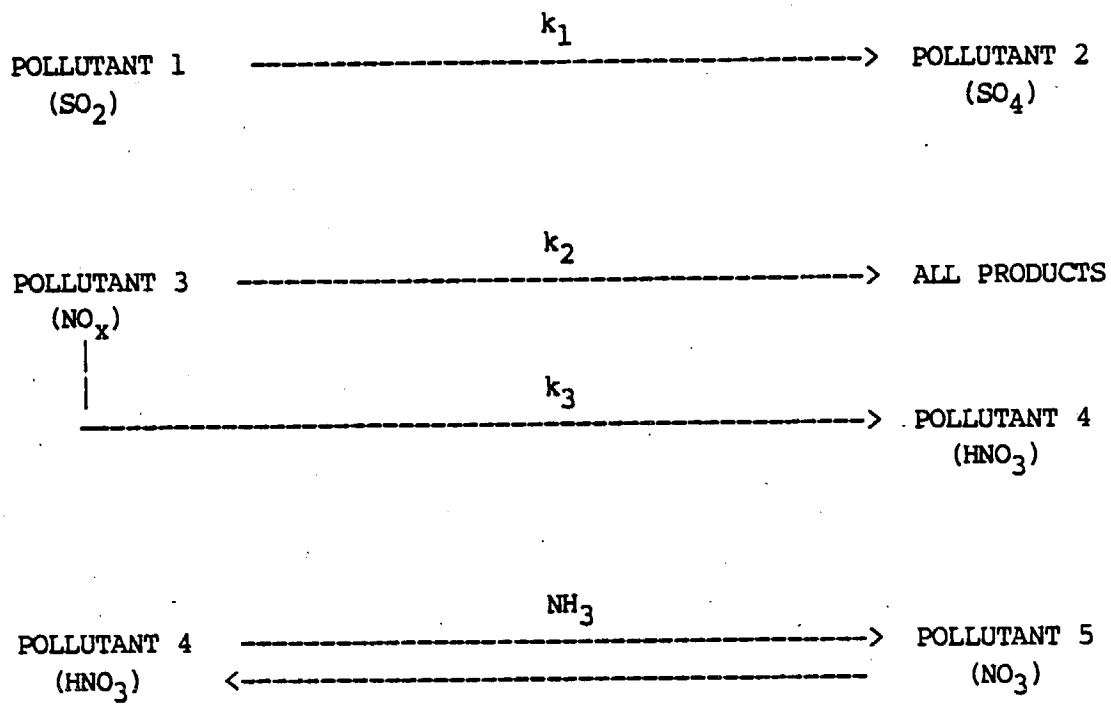

Figure 5.8-4. Schematic representation of chemical pathways in the five-pollutant Mechanism 1 system.

5.9 Wet Removal

Many studies have shown that during rain events, wet scavenging of soluble or reactive pollutants can be of the order of tens of percent per hour (Barrie, 1981; Slinn et al., 1978; Levine and Schwartz, 1982; Scire and Venkatram, 1985). Gaseous pollutants are scavenged by dissolution into cloud droplets and precipitation. For SO_2, aqueous-phase oxidation can be an important removal pathway. Particulate pollutants are removed by both in-cloud scavenging (rainout) and below-cloud scavenging (washout). Over source-receptor distances of tens to hundreds of kilometers, wet scavenging can deplete a substantial fraction of the pollutant material from the puff.

Scott (1978, 1981) has found precipitation scavenging of sulfate to be a function of the mechanism of precipitation formation and storm type (Figure 5.9-1). For example, the ratio of sulfate concentration in precipitation to that in air (i.e., the washout ratio, W) is 10-50 times larger for precipitation with growth due primarily to accretion than for precipitation growth due to vapor deposition. Slinn et al. (1978) note that snow scavenging of gases is generally negligible. The scavenging efficiency of SO_2 is a function of the pollutant solubility in water and reactivity. Barrie (1981) relates the SO_2 washout ratio to the pH and temperature (Figure 5.9-2).

Due to concerns of the effects of acid deposition, detailed cloud and aqueous-phase chemistry modules (e.g., Karamanchandani et al., 1985; NCAR, 1985) have been developed for the wet removal of sulfur and nitrogen compounds. However, this level of detail is impractical and unncessary for the proposed model. A simple approach that has been shown (e.g., Maul, 1980) to yield realistic long-term estimates of wet removal is the empirically-based scavenging coefficient method. The depletion of a pollutant is represented as:

$$C_{t+dt} = C_t \exp[-\Lambda dt] \qquad (5.9\text{-}1)$$

where C is the concentration (g/m^3) at time t and t + dt, and,
Λ is the scavenging ratio.

The scavenging ratio can be expressed as:

$$\Lambda = \lambda (R/R_1) \qquad (5.9\text{-}2)$$

where λ is the scavenging coefficient,
R is the precipitation rate (mm/hr), and,
R_1 is a reference precipitation rate of 1 mm/hr.

The scavenging ratio depends on the characteristics of the pollutant

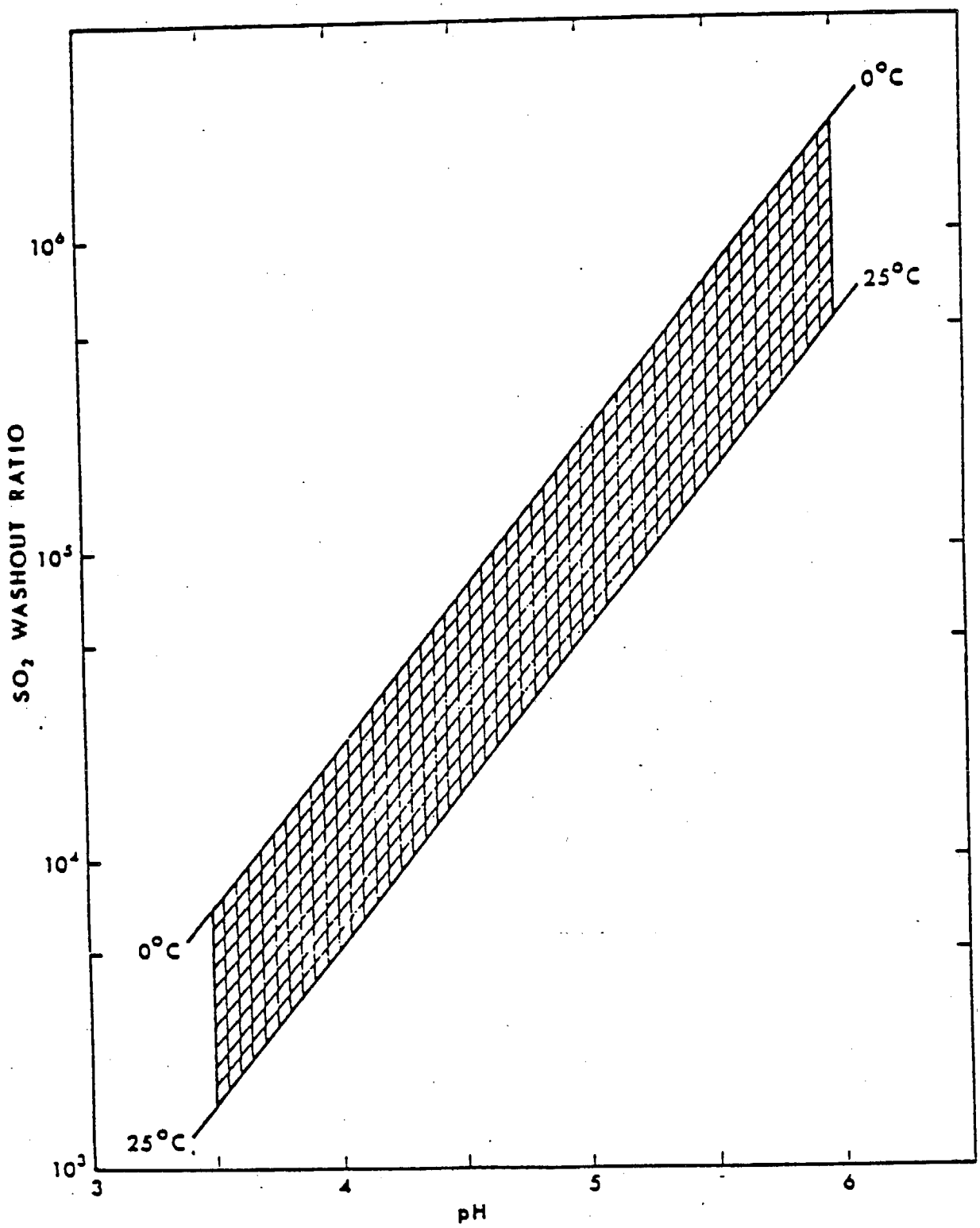

Figure 5.9-2. SO_2 Washout Ratio as a Function of pH and Temperature for Equilibrium Scavenging Conditions. [From Barrie (1981)].

6. Postprocessor Programs

Two postprocessing programs will be provided as part of the modeling system. The first program provides for the processing, analysis, and display of the concentration or wet and dry flux output of the dispersion model. The second program is intended to allow the user access to user-selected portions of the very large quantity of meteorological output that will be prooduced by the meteorological model. This section described the major features of these two programs.

The structure of the concentration/flux postprocessor program is based on the MESOFILE II postprocessor program for the MESOPUFF II model. The program consists of a number of subroutines that perform various data processing operations on the gridded or nongridded model output fields. Selection of a processing operation is made by the placement by the user of keywords in the postprocessor's input file. The capabilities of the various routines and their keywords are described below.

FIXAVE - This routine performs block-average calculations of gridded or nongridded model output fields for a user-specified averaging time. The routine contains options for tabular output (gridded or nongridded receptors), line printer plots (gridded receptors only), or disk output. Scaling factors can be applied.

RUNAVE - This routine performs running-average calculations of gridded or nongridded model output fields for a user-specified averaging time. The routine contains options for tabular output (gridded or nongridded receptors), line printer plots (gridded receptors only), or disk output. Scaling factors can be applied.

SEQADD - SEQADD adds the results of up to five separate model output files. The results can be displayed in tabular form, plotted, or stored on disk. Separate scaling factors can be applied to each of the five input files.

INTEGR - This routine sums the results from one model run in time (e.g., to compute time-integrated total deposition). The results can be displayed in tabular form, plotted, or stored on disk. Scaling factors can be applied.

STAT - The STAT routine performs statistical analysis of point-by-point or bulk differences between two gridded concentration or deposition fields. The statistics computed include the mean of each field, mean deviation, mean absolute deviation, difference of maxima, correlation coefficient, and fractional deviation statistics. The difference fields or fractional difference fields can be displayed

REFERENCES

Arya, S.P.S., 1984. Parametric Relations for the Atmospheric Boundary Layer. Bound. Layer Meteor., 30, 57-73.

Atkinson, R., A.C. Lloyd, and L. Winges, 1982. An Updated Chemical Mechanism for Hydrocarbon/NO_x/SO_x Photooxidation Suitable for Inclusion in Atmospheric Simulation Models. Atmospheric Environment, 16, 1341.

Barad, M.L. (ed.), 1958. Project Prairie Grass: A Field Program in Diffusion. Geophysical Research Papers, No. 59, Vols. I and II, AFCRF-TR-58-235, Air Force Cambridge Research Center, Bedford, MA.

Barrie, L.A., 1981. The Prediction of Rain Acidity and SO_2 Scavenging in Eastern North America. Atmospheric Environment, 15, 31-41.

Benkley, C.W. and A. Bass, 1979. Development of Mesoscale Air Quality Simulation Models. Volume 2. User's Guide to MESOPLUME (Mesoscale Plume Segment) Model. EPA-600/7-79-xxx. U.S. Environmental Protection Agency, Research Triangle Park, NC.

Benkley, C.W. and L.L. Schulman, 1979. Estimating Hourly Mixing Depths from Historical Meteorological Data. J. Appl. Meteor., 18, 772-780.

Berkowicz, R. and L.P. Prahm, 1982. Evaluation of the Profile Method for Estimation of Surface Fluxes of Momentum and Heat. Atmospheric Environment, 16, 2809-2819.

Binkowski, F.S., 1979. A Simple Semi-Empirical Theory for Turbulence in the Atmospheric Surface Layer. Atmospheric Environment, 13, 247-253.

Blackadar, A.K. and H. Tennekes, 1968. Asymptotic Similarity in Neutral Barotropic Planetary Bounday Layers. J. Atmos. Sci., 25, 1025-1020.

Bowers, J.F. and A.J. Anderson, 1981. An Evaluation Study for the Industrial Source Complex (ISC) Dispersion Model. EPA 450/4-81-002, U.S. Environmental Protection Agency, Research Triangle Park, NC.

Bowers, J.F., J.R. Bjorklund and C.S. Cheney, 1979. Industrial Source Complex (ISC) Dispersion Model User's Guide. Volume I. EPA-450/4-79-030. U.S. Environmental Protection Agency, Research Triangle Park, NC.

Briggs, G.A., 1973. Diffusion Estimates for Small Emissions (Draft). Air Resources Atmospheric Turbulence and Diffusion Laboratory. ATOL No. 79.

Deardorff, J.W. and G.E. Willis, 1975. A parameterization of diffusion into the mixed layer. J. Appl. Meteor., 14, 1451-1458.

Deardorff, J.W. and G.E. Willis, 1982. Ground-Level Concentrations Due to Fumigation into an Entraining Mixed-Layer. Atmospheric Environment, 16, 1159-1170.

DeBruin, H.A.R., and A.A.M. Holtslag, 1982. A Simple Parameterization of the Surface Fluxes of Sensible and Latent Heat During Daytime Compared with the Penman-Monteith Concept. J. Appl. Meteor., 21, 1610-1621.

DiCristofaro, D.C., D.G. Strimaitis, B.R. Greene, R.J. Yamartino, A. Venkatram, D.A. Godden, T.F. Lavery, B.A. Egan, 1985. EPA Complex Terrain Model Development Program: Fifth Milestone Report - 1985. EPA-600/3-85/069, U.S. Environmental Protection Agency, Research Triangle Park, NC.

Draxler, R.R., 1976. Determination of Atmospheric Diffusion Parameters. Atmospheric Environment, 10, 99-105.

Draxler, R.R., 1984. Diffusion and Transport Experiments. In Atmospheric Science and Power Production, D. Randerson, Ed. DOE/TIC-27601, NTIS, Springfield, VA.

Drazin, P.G., 1961. On the Steady Flow of a Fluid of Variable Density Past an Obstacle. Tellus, 13, 239-251.

Dumbauld, R.K., J.C. Rafferty and H.E. Cramer, 1976. Dispersion-deposition from Aerial Spray Releases. Preprint Volume for the Third Symposium on Atmospheric Diffusion and Air Quality, American Meteorological Society, Boston, MA.

Forrest, J., R.W. Garber and L. Newman, 1981. Conversion Rates in Power Plant Plumes Based on Filter Pack Data: The Coal-fired Cumberland Plume. Atmospheric Environment, 15, 2273.

Fowler, D. and M.H. Unsworth, 1979. Turbulent transfer of sulphur dioxide to a wheat crop. Q.J. Roy. Meteor. Soc., 105, 767-784.

Godowitch, J.M., J.K.S. Ching, and J.F. Clarke, 1981. Urban/Rural and Temporal Variations in PBL Turbulence Parameters and Length Scales over St. Louis, MO. AMS Fifth Symposium on Turbulence, Diffusion, and Air Pollution, March 9-13, Atlanta, GA.

Golder, D., 1972. Relations Among Stability Parameters in the Surface Layer. Bound. Layer Met., 3, 46-58.

Hosker, R.P., Jr. and S.E. Lindberg, 1982. Review: Atmospheric Deposition and Plant Assimilation of Gases and Particles. Atmospheric Environment, 16, 889-910.

Hosker, R.P., 1984. Flow and Diffusion Near Obstacles. In Atmospheric Science and Power Production. R. Randerson, Ed. DOE/TIC-27601. National Technical Information Service, Springfield, Virginia.

Huber, A.H. and W.H. Snyder, 1982. Wind Tunnel Investigation of the Effects of a Rectangular-Shaped Building on Dispersion of Effluents from Short Adjacent Stacks. Atmospheric Environment, 17, 2837-2848.

Hunt, J.C.R., 1982. Diffusion in the Stable Boundary Layer. In Atmospheric Turbulence and Air Pollution Modeling. F.T.M. Nieuwstadt and H. van Dop, Eds. D. Reidel Publishing Co., Boston, MA.

Hunt, J.C.R. and W.H. Snyder, 1980. Experiments on Stably and Neutrally Stratified Flow over a Model Three-Dimensional Hill. J. Fluid Mech., 96, 671-704.

Hunt, J.C.R., J.S. Puttock, and W.H. Snyder, 1979. Turbulent Diffusion from a Point Source in Stratified and Neutral Flows Around a Three-Dimensional Hill (Part I - Diffusion Equation Analysis). Atmospheric Environment, 13, 1227-1239.

Hunt, J.C.R. and R.J. Mulhearn, 1973. Turbulent Dispersion from Sources Near Two-Dimensional Obstacles. J. Fluid Mech., 61, 245-274.

Irwin, J.S., 1979. Scheme for Estimating Dispersion Parameters as a Function of Release Height. EPA-600/4-79-062. U.S. Environmental Protection Agency, Research Triangle Park, NC.

Irwin, J.S., 1983. Estimating Plume Dispersion - A Comparison of Several Sigma Schemes. J. Clim. and Appl. Meteor., 22, 92-114.

Karamchandani, P., F. Lurmann, and A. Venkatram, 1985. ADOM/TADAP Model Development Program. Volume 8: Central Operator. Ontario Ministry of the Environment, Toronto, Ontario, Canada.

Kerman, B.R., 1982. A Similarity Model of Shoreline Fumigation. Atmospheric Environment, 16, 467-477.

Kitaigorodskii, S.A., 1973. The Physics of Air-Sea Interaction. Israel Program for Scientific Translations. Jerusalem.

Oke, T.R., 1982. The Energetic Basis of the Urban Heat Island. Quart. J. R. Met. Soc., 108, 1-24.

Panofsky, H.A., H. Tennekes, D.H. Lenschow, J.C. Wynngaard, 1977. The Characteristics of Turbulent Velocity Components in the Surface Layer Under Convective Conditions. Bound. Layer Meteor., 11, 355-361.

Pasquill, F., 1976. Atmospheric Dispersion Parameters in Gaussian Plume Modeling: Part II. Possible Requirements for Change in the Turner Workbook Values. EPA-600/4-76-030b, U.S. Environmental Protection Agency, Research Triangle Park, No. Carolina. 53 pp.

Peterson, W.B., 1986. A Demonstration of INPUFF with the MATS Data Base. Atmospheric Environment, 20, 1341-1346.

Pierce, T.E and D.B. Turner, 1980. User's Guide for MPTER. EPA-600/8-80-016. U.S. Environmental Protection Agency, Research Triangle Park, NC.

Pleim, J., A. Venkatram and R.Y. Yamartino, 1985. ADOM/TADAP Model Development Program. Volume 4. The Dry Deposition Model. Ontario Ministry of the Environment, Rexdale, Ontario, Canada.

Raynor, G.S., S. SethuRaman, R.M. Brown, 1979. Formation and Characteristics of Coastal Internal Boundary Layers During Onshore Flow. Bound. Layer Meteor., 16, 487-514.

Riley, J.J., Liu, H.T. and Geller, E.W., 1976. A Numerical and Experimental Study of Stably Stratified Flow Around Complex Terrain, EPA Report No. EPA-600/4-76-021, Res. Tri. Pk., NC, 41 p.

Rittmann, B.E., 1982. Application of the Two-Thirds Law to Plume Rise from Industrial-Sized Sources. Atmospheric Environment, 16, 2575-2579.

Schulman, L.L. and J.S. Scire, 1980. Buoyant Line and Point Source (BLP) Dispersion Model User's Guide. Document P-7304-B. Environmental Research & Technology, Inc., Concord, MA.

Schulman, L.L. and J.S. Scire, 1981. The Development and Capabilities of the BLP Model. In Proceedings APCA Specialty Conference on Dispersion Modeling from Complex Sources. St. Louis.

Schulman, L.L. and S.R. Hanna, 1986. Evaluation of Downwash Modifications to the Industrial Source Complex Model. JAPCA, 36, 258-264.

Slinn, W.G.N., L. Hasse, B.B. Hicks, A.W. Hogan, D. Lal, P.S. Liss, K.O. Munnich, G.A. Sehmel, and O. Vittori, 1978. Some aspects of the transfer of atmospheric trace constituents past the air-sea interface. Atmospheric Environment, 12, 2055-2087.

Snyder, W.H., R.E. Britter and J.C. R. Hunt, 1980. A Fluid Modeling Study of the Flow Structure and Plume Impingement on a Three-Dimensional Hill in Stably Stratified Flow. Proc. Fifth Int. Conf. on Wind Engr. (J.E. Cermak, ed.), 1: 319-329, Pergamon Press, New York, NY.

Snyder, W.H. and J.C.R. Hunt, 1984. Turbulent Diffusion from a Point Source in Stratified and Neutral Flow Around a Three-Dimensional Hill (Part II - Laboratory Measurement of Surface Concentrations). Atmospheric Environment, 18, 1969-2002.

Stelson, A.W., and J.H. Seinfeld, 1982. Relative Humidity and Temperature Dependence of the Ammonium Nitrate Dissociation Constant. Atmospheric Environment, 16, 983-992.

Stelson, A.W., M.E. Bassett and J.H. Seinfeld, 1983. Thermodynamic Equilibrium Properties of Aqueous Solutions of Nitrate, Sulfate and Ammonium. Acid Precipitation, Chemistry of Particles, Fog and Rain. J. Teasley, ed. Ann Arbor Science, Woburn, MA.

Strimaitis, D.G., T.F. Lavery, A. Venkatram, D.C. DiCristofaro, B.R. Greene, and B.A. Egan, 1984. EPA Complex Terrain Model Development Program: Fourth Milestone Report - 1984. EPA-600/3-84-110, U.S. Environmental Protection Agency, Research Triangle Park, NC.

Stunder, M. and S. SethuRaman, 1985. A Comparative Evaluation of the Coastal Internal Boundary Layer Height Equations. Bound. Layer Meteor., 32, 177-204.

Thuiller, R.H., 1982. Dispersion Characteristics in the Lee of Complex Structures. JAPCA, 32, 526-532.

Unsworth, M.H. and J.L. Monteith, 1972. Aerosol and Solar Radiation in Britain. Quart. J.R. Met. Soc., 98, 778-797.

Van Egmond, N.D., and H. Kesseboom, 1983. Mesoscale Air Pollution Dispersion Models - II. Lagrangian Puff Model and Comparison with Eulerian Gird Model. Atmospheric Environment, 17, 267-274.

Van Ulden, A.P. and A.A.M. Holtslag, 1985. Estimation of Atmospheric Boundary Layer Parameters for Diffusion Applications. J. Clim. and App. Meteor., 24, 1196-1207.

CARB LIBRARY
06246

Yamartino, R.J., P.G. Luehring, and R.M. Stern, 1979. Analysis of several low wind speed tracer experiments. Proc. of the NATO/CCMS 10th Int. Tech. Meeting on Air Poll. Modeling and its Applications, Rome, Italy, 325-338.

Zannetti, P., 1981. An Improved Puff Algorithm for Plume Dispersion Simulation. J. Appl. Meteor., 20, 1203-1211.